A comparison of earthwork designs for railway transition zones

Chumyen, P.; Connolly, D. P.; Woodward, P. K.; Markine, V.

DOI
10.1016/j.conbuildmat.2023.132295

Publication date
2023

Document Version
Final published version

Published in
Construction and Building Materials

Citation (APA)
Chumyen, P., Connolly, D. P., Woodward, P. K., & Markine, V. (2023). A comparison of earthwork designs for railway transition zones. *Construction and Building Materials*, *395*, Article 132295. https://doi.org/10.1016/j.conbuildmat.2023.132295

Important note
To cite this publication, please use the final published version (if applicable).
Please check the document version above.

Construction and Building Materials 395 (2023) 132295

Contents lists available at ScienceDirect

Construction and Building Materials

journal homepage: www.elsevier.com/locate/conbuildmat

A comparison of earthwork designs for railway transition zones

P. Chumyen [a,*], D.P. Connolly [a,*], P.K. Woodward [a], V. Markine [b]

[a] School of Civil Engineering, University of Leeds, LS2 9JT, UK
[b] Delft University of Technology, Delft, The Netherlands

ARTICLE INFO

Keywords:
Railway Transition Earthworks
Ground improvement
Embankment-Bridge transition zones
Railroad dynamics
Wedge-shaped soil reinforcement

ABSTRACT

Railway track transitions are zones where there is an abrupt change in the track-ground structure. They are often the location of rapid track deterioration, which means more frequent track maintenance is needed compared to plain line tracks. With the aim of reducing maintenance, modern transition zone designs use tapered stiffness earthwork profiles to minimise train-track dynamics. However, there has been limited comparison regarding the effect of different tapered profiles on dynamic behaviour. Therefore, this paper's novelty is the investigation of the performance of different earthwork designs in smoothing stiffness transition's considering different types of improvement and also train speed. To do so, first a 3D finite element track model is developed, with support conditions transitioning from an earth embankment onto a concrete bridge. A dynamic moving train load is simulated using a rigid multi-body approach capable of accounting for train-track interaction. The model is used to study the effect of four earthwork solutions with differing stiffness tapers. For each scenario, two different track structure types (ballast and concrete slab) are considered, along with different magnitudes of ground improvement. Lastly, the effects of train speed are explored. It is found tapered earthwork solutions for ballasted tracks show greater dynamic improvement compared to slabs due to their reduced bending stiffness. Further, the more complex improvement geometries such as double trapezoid shapes offer some additional improvement at locations within 3 m of the bridge. However, when considering such tapered stiffness-based earthwork solutions, additional factors such as constructability must also be considered.

1. Introduction

Railway embankments play an important role in providing a stable foundation for track structures during repeated train passages, as well as assisting with drainage and vertical rail alignment. They are located below the track-bed layers (ballast, sub-ballast, and capping layer) and are constructed from earth material [1]. Although embankment construction materials are highly engineered, they inherently have lower stiffness than bridge structures which are typically formed from steel or concrete [2]. This rapid change in stiffness along the track can result in differential track settlement and dynamic wave propagation [3,4] due to differing track stiffness [5–8]. These effects can reduce transition zone lifespan [9], passenger comfort and ride quality [10,11] and result in maintenance interventions up to six times more frequent than on plain line [12]. Therefore, it can be beneficial to minimise these effects by carefully optimising the stiffness along the track section.

One method for improving track performance at transitions is using pile-type structures made from stone columns, reinforced concrete, or steel which have been shown to improve embankment stiffness and reduced track settlement [13–16]. For example, [17] performed field tests and numerical simulations of an embankment-bridge transition with a pile group and geogrid. The field data and numerical results indicated the combined solution of pile and geogrid could gradually change subgrade displacement between the embankment and bridge. However, the installation and maintenance of piling can be complicated and costly, depending on the pile material and length [5,13]. Its effectiveness relies on pile type, diameter, and installation pattern [18].

Geosynthetic materials such as geogrid and geotextile can help increase the bearing capacity of soil [19] and the elastic shakedown load limit [20]. Although some studies suggest using geogrid provides better track transition performance [21,22], some findings from numerical studies in [23] and [24] indicate geogrid does not significantly improve settlement. The performance of the grid depends on various factors such as depth, soil strength parameters, and loading-induced elastic stresses. Other solutions to improve track support performance include approach slabs [25], transition modules [26], and hot mix asphalt [27,28] which

* Corresponding authors.
E-mail addresses: ml16p3c@leeds.ac.uk (P. Chumyen), d.connolly@leeds.ac.uk (D.P. Connolly).

https://doi.org/10.1016/j.conbuildmat.2023.132295
Received 1 March 2023; Received in revised form 24 May 2023; Accepted 23 June 2023
Available online 1 July 2023

reduce the stresses acting in the soil [24]. Nevertheless, issues related to their lifespan and long-term performance are still reported in transition studies [24,29].

In addition to modifying the track-bed structure at existing transitions, soil reinforcement using wedge shapes is a common design feature of the underlying earthworks. These designs typically attempt to taper the earthwork stiffness across the transition using high-stiffness materials such as cement-bound mixture (CBM) or unbound granular material (UGM) [5]. Different railway administrations use them in various forms for bridge transition design, as shown in Fig. 1. In 1978, the Japanese National Railways introduced an approaching block of trapezium-shaped (Type A: Single trapezoid) backfill behind the abutment, where the original backfill was replaced with well-compacted and graded gravel [30,31]. Additionally, three forms of bridge transition (Type A: Single trapezoid, Type C: Single trapezoid (inverted) and Type D: Double trapezoid (inverted)) were recommended in design codes for railway embankments [32,33] Another design has been proposed in on European railway lines, such as DB (Germany), ADIF (Spain), SNCF (France) and REFER (Portugal), which is composed of two parts of a trapezoid (Type B: Double trapezoid (inverted)) [12,34].

The different earthwork approaches within standards indicate a lack of consensus in earthwork designs for embankment-bridge transitions. Therefore, studies have been performed to investigate asset performance, considering track behaviour of each of these forms, as summarised in Table 1. However, their conclusions are mostly based on single track-forms spanning the transition length. Few studies have extended such analysis to varying track-forms over the length, for example, comparing a ballasted track on both embankment-bridge to a ballasted track on the embankment transitioning to a slab track on the bridge.

Multiple studies have proposed numerical approaches to study transition zones, with some solely using 2D Finite element (FE) modelling [36,41,42,43]. Although these models allow for simulation with minimal computational effort compared to 3D models, they do not capture the 3D stress wave propagation induced by the dynamics at the transition [44]. Additionally, this can make it challenging to calculate the 3D deviator stress, which can be used for track settlement analysis [2,45,46].

3D FE modelling can overcome the problems above [47] and has received significant attention [48,49] as discussed in [13]. Its versatility in simulating complex geometries allows it to solve problems related to track-soil coupling and deep soil wave propagation [49], including earthwork solutions at embankment-bridge transitions [17,37,39]. Other advanced simulation approaches include the use of coupled discrete element (DEM) and finite difference methods (FDM). This is where DEM is used to model the sleeper and ballast particles and FDM for the abutment, transition, and embankment [38]. Further, the coupling of DEM and computational fluid dynamics (CFD) has been developed to investigate soil deformation when the seepage flow increases (approaching fluidisation) under the track. To do this, the soil particles are modelled using DEM while the fluid flow is simulated using CFD [50]. However, the complexity of these coupled modelling approaches is high, with potentially long computational times, meaning transition zone domains typically require truncation, potentially resulting in track lengths insufficient for transition study.

Due to the lack of consensus for standard design, this paper aims to investigate and compare the performance of earthwork solutions for various track transition forms over an embankment-bridge transition length. To achieve this, a 3D FE approach is used, considering the dynamic response due to train-track interaction. The model incorporates perfectly matched layers (PML) for absorbing boundaries and is solved explicitly in the time domain, while treating the vehicle as a multi-body system. The analysis examines the dynamic behaviour of different earthwork material stiffnesses and configurations, subject to varying train speeds. As a result, it provides a novel contribution to the field of earthwork solutions for railway bridge approaches.

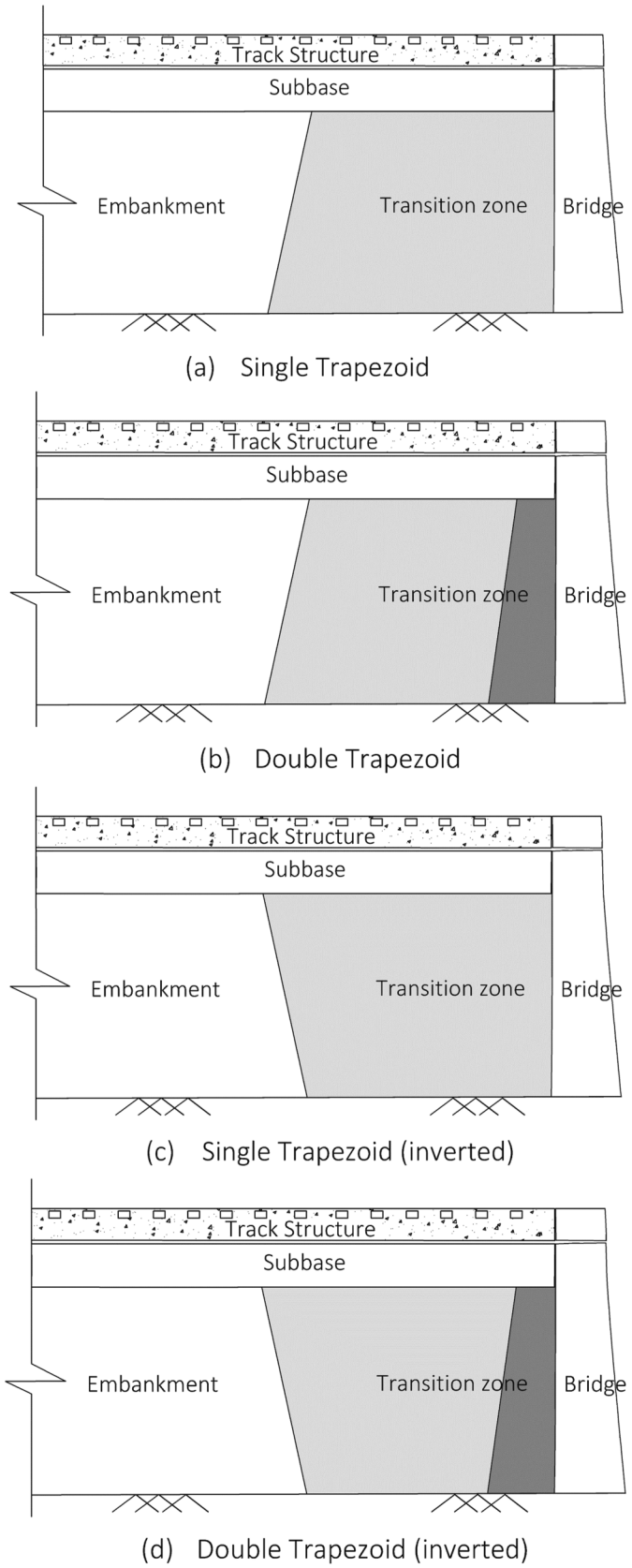

Fig. 1. Example transition zone earthwork configurations.

Table 1
Summary of earthwork solutions at railway transition zones.

Author	Earthwork configuration(s) (Fig. 1)	Description
[17]	Type A: Single trapezoid Type C: Single trapezoid (inverted)	• Developed the 3D FE modelling to analyse earthwork solutions using graded gravel plus 5% of cement, piling, and geogrid. • Studied the transition from a ballasted track on the embankment to a slab track on the bridge. • The type C configuration provided an improved dynamic stress behaviour compared to type A. • The recommended length to stiffen the transition was 18 to 30 m from the abutment.
[35]	Type A: Single trapezoid Type C: Single trapezoid (inverted)	• Developed the 3D FE modelling to investigate the influence of train speed, material stiffness and earthwork configuration on the dynamic response of the bridge approach. • Studied the transition from a slab track on the embankment to a slab track on the bridge. • The earthwork solution was constructed next to the abutment using fibre-reinforced light-weight concrete (FRLWC). • The type C configuration provided improved track performance regarding displacement and acceleration compared to type A.
[36]	Type B: Double trapezoid	• Developed the 2D FE modelling of bridge transition and performed field measurements to investigate track stiffness and displacement at the embankment-bridge transition after applying the earthwork solution. • The solution consisted of the CBM (Cement Bound Material) located next to the bridge and the unbound granular material (graded crushed limestone aggregate) placed between the CBM and the embankment. • Studied the transition from a ballasted track on the embankment to a ballasted track on the bridge. • The type B configuration resulted in a smoother change in track stiffness and displacement.
[37]	Type C: Single trapezoid (inverted) Type D: Double trapezoid (inverted)	• Developed the 3D FE modelling to investigate and compare the dynamic track behaviour of two types of earthwork configurations: C and D. • The transition zone for Types C and D utilised graded coarse-grained soil, and for Type D, graded broken stone was added behind the bridge. • Studied the transition from a slab track on the embankment to a slab track on the bridge. • A recommended total transition length is 30 m. • The type D configuration show improvements in track displacement, stress and acceleration compared to type C.
[38]	Type A: Single trapezoid Type B: Double trapezoid Type C: Single trapezoid (inverted) Type D: Double trapezoid (inverted)	• Developed the DEM-FDM coupling model to evaluate the dynamic track performance of different earthwork configurations. • Studied the transition from a ballasted track on the embankment to a ballasted track on the bridge. • The type C and D configurations provided better track performance compared to types A and B. • The track performances of the double transition form (Type B and D) were better than the single form (Type A and C). • Increasing the elastic modulus of the transition section can significantly affect track displacement, although the effect becomes minor when the modulus exceeds 2500 MPa.
[39]	Type A: Single trapezoid Type C: Single trapezoid (inverted)	• Developed the 3D FE modelling to consider the design factors of an embankment-bridge transition constructed with granular material. • Studied the transition from a ballasted track on the embankment to a ballasted track on the bridge. • A slope (Horizontal: Vertical) of 1:1 was recommended for the earthwork solution. • Based on the investigated material properties, a value of 25 MPa was suggested for the transition zones.
[40]	Type C: Single trapezoid (inverted)	• Developed the 2D FE modelling to optimise the transition zones based on the deterministic and robust design principles. • Studied the transition from a slab track on the embankment to a slab track on the bridge. • Stress amplification was observed in the area adjacent to the bridge, which should be considered in the design of stiffness combination. • The optimal stiffness value for the subgrade bed surface layer and the graded broken stone area were determined as 1200 MPa and 1000 MPa, respectively.

2. Numerical modelling

A finite element model is developed to study the dynamic response of transition zones. The pre-processing, including meshing and input file generation, is performed using MATLAB before being solved using commercial FE software LS-DYNA. The components of the model, which include the vehicle, track, soil, and bridge, are described below.

2.1. Embankment-Bridge transition model

The underlying transition zone spans across an earthwork embankment onto a concrete bridge deck. The following permutations of track structure spanning the structure are considered:

1) Ballasted track on both embankment and bridge
2) Ballasted track on the embankment, with slab track on the bridge
3) Concrete slab track on both embankment and bridge

Both tracks consist of discretely supported rails. Fig. 2 presents the ballasted track components, including sleepers, ballast, and sub-ballast. The slab track comprises a concrete slab, a hydraulically bonded layer (HBL) and a frost protection layer (FPL), as shown in Fig. 3. Further, a subbase is placed beneath the sub-ballast for the ballasted track and beneath the FPL for the slab track.

All elements are fully integrated eight-node solid hexahedral elements. In the Cartesian coordinate system, the X, Y, and Z axes represent the longitudinal, vertical, and lateral directions, respectively. Element size is defined by the relationship between wavelength, frequency, and shear wave speed [51]. The maximum mesh size in X, Y and Z axes are 0.2 m, 0.3 m and 0.2 m, respectively. Additionally, earthwork transition solutions are placed between the standard embankment and the bridge abutment, as shown in Fig. 4. Full coupling is used across all component interfaces.

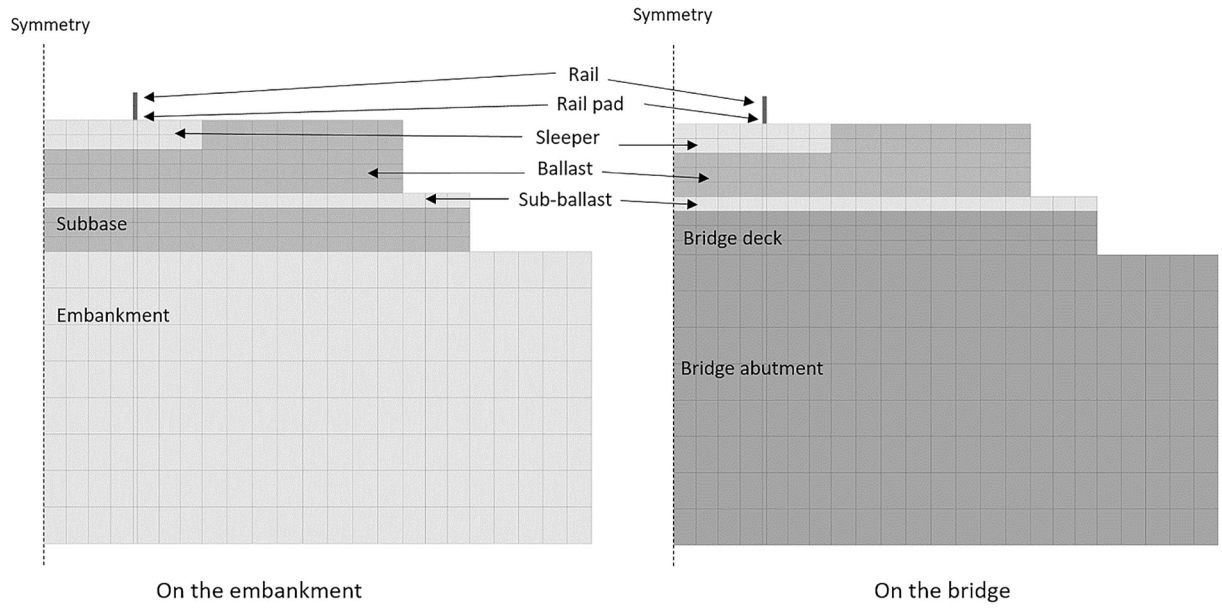

Fig. 2. Ballasted track configuration on both the embankment and bridge.

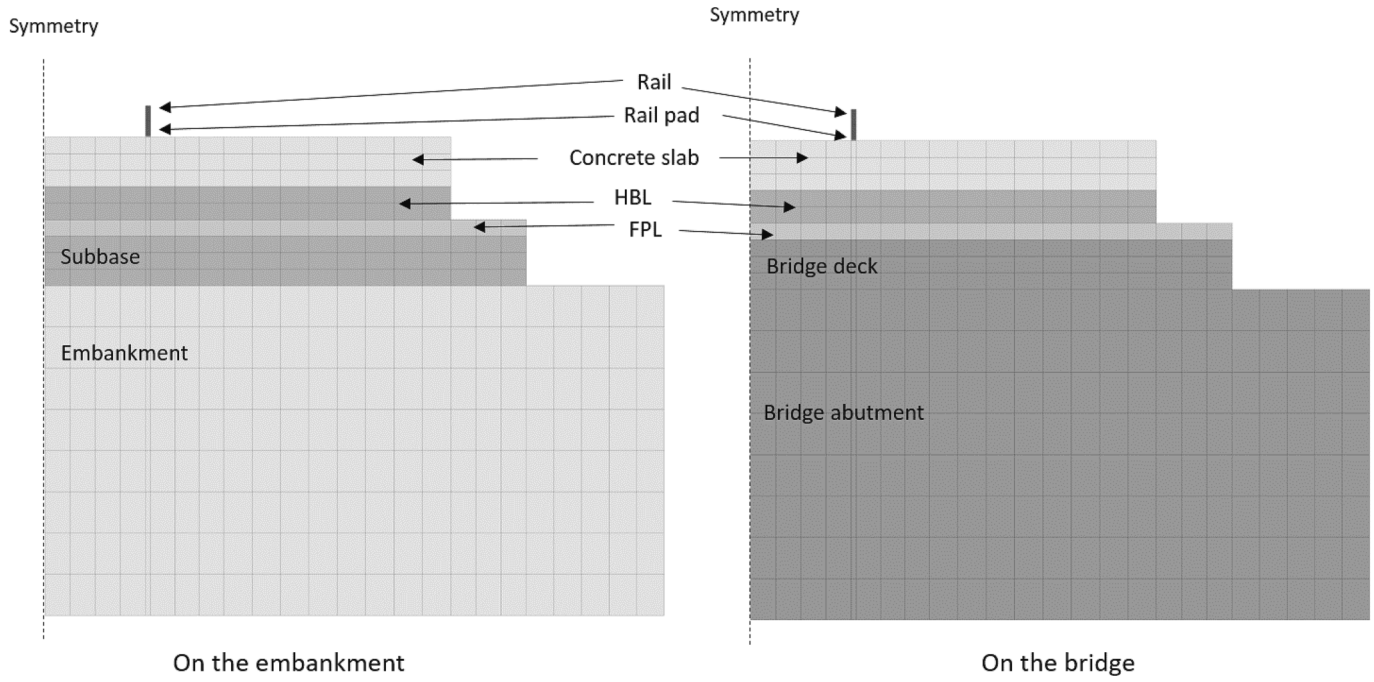

Fig. 3. Slab track configuration on both the embankment and bridge.

2.2. Material properties and boundary conditions

The material behaviour for all components is assumed to be isotropic and linear elastic, which means track displacements are limited to the elastic range of the stress–strain curve. To define track-ground interaction, four material properties are considered: density, Young's modulus, Poisson's ratio, and damping. An equivalent modulus is used to convert the more commonly used rail pad vertical spring stiffness into solid element modelling, based on the relationship between the rail pad dimensions and Poisson's ratio [52]. Further, the damping properties are determined using Rayleigh damping coefficients, which are related to the mass and stiffness matrices and estimated based on the relationship between the damping ratio and circular frequency [53,54].

Regarding the domain boundary conditions, symmetry is implemented in the vertical plane (at Z = 0 m) of the track, embankment, and bridge [55]. PML is employed to absorb wave energy and is placed at the boundaries of the soil [56], as shown in Fig. 5. Fixed constraints are applied to the outer surfaces of the PML, the bottom surfaces of the bridge abutment, and both ends of the track model.

2.3. Vehicle modelling

The vehicle model is an extension of the approach proposed in [57]. It is a multi-body system consisting of one car body, two bogies and four wheelsets, all moving at a constant speed. The model also includes primary and secondary suspension systems and vehicle-track

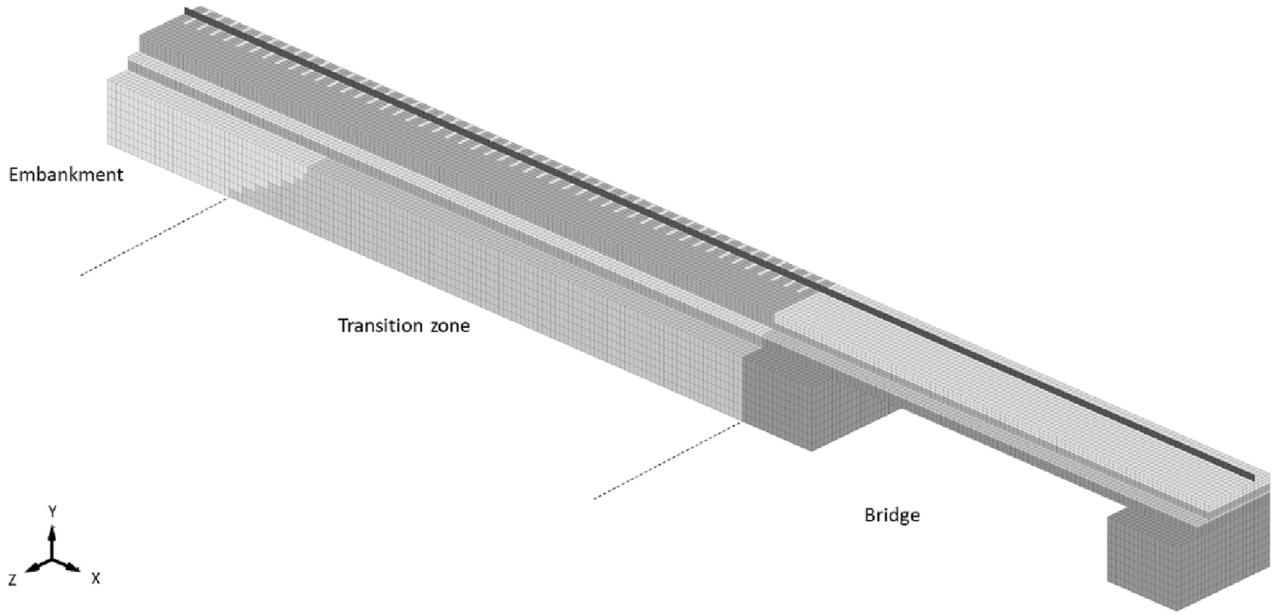

Fig. 4. Numerical modelling domain (embankment length truncated for viewability).

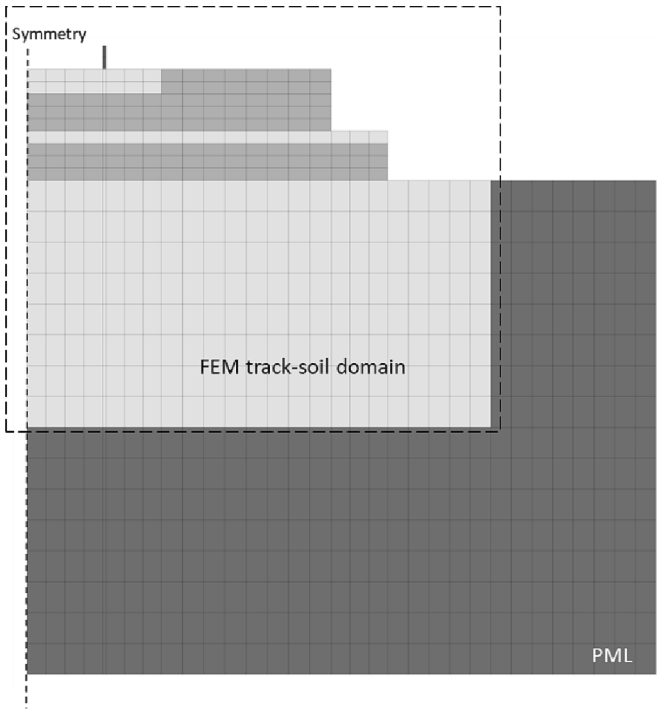

Fig. 5. Absorbing boundaries of soil structure using the PML approach.

interaction, as shown in Fig. 6.

The car body is modelled using 2D shell elements with rigid body mass (M_c) and pitching moment of inertia (I_c). The bogies are modelled using beam elements with distributed mass (M_b) and pitching moment of inertia (I_b) while the wheelset is modelled as a concentrated mass (M_w). Spring-damper sets are used to represent the primary (k_p,c_p) and secondary (k_s,c_s) suspensions, located between the wheelsets-bogies and car body-bogies, respectively.

For the vehicle-track interaction, Hertzian contact theory is employed with a stiffness value (k_H). Since the static action (i.e., the dead load of a vehicle) has a significantly larger impact on the contact force than the dynamic portion, the contact stiffness can be linearised using the procedure proposed in [58]. As the wheelset and rail are made of similar steel material, the linearized (Hertzian) vehicle-track coupling is defined using Equation (1):

$$kH = \sqrt[3]{\frac{3f_s r_{eq} E_s^2}{2(1-v_s^2)^2}} \quad (1)$$

where f_s is the static load per wheel (N), r_{eq} represents the equivalent circular contact surface (m) of wheel radius (R_{wheel}) and rail curvature (R_{rail}), in which $req = \sqrt{R_{wheel} \times R_{rail}}$, E_s and v_s are Young's modulus of elasticity and Poisson's ratio of steel, respectively.

Then, the wheel node and rail surface are defined as slave and master segments for the moving load simulation using the penalty contact method. Rather than using the default value provide LS-DYNA software, the Hertzian stiffness is obtained to represent the force at the master segment when penetration is detected [59]. This force moves the penetrating node back to the rail surface and reduces numerical instabilities [55].

2.4. Model solver and validation

The simulation process is performed in two phases: static, followed by dynamic. A relaxation technique [55,60] is applied during the initial static analysis to determine the initial boundary conditions of the vehicle-track-ground system. After the static phase, moving dynamic train loading begins. This transient dynamic analysis computes the track response based upon time-dependent train-track interaction. The problem is solved using explicit integration with a time step of 4.94×10^{-6} s. The modelling approach has previously been validated with the field measurement data as presented in [57].

3. Simulation parameters

An earthwork solution with a stiffness of 400 MPa (representing an UGM with graded gravel plus 3% of cement) and a single trapezoid (inverted) form (Type C in Fig. 1) with a moving vehicle at 212 km/hr speed serves as the benchmarks for all investigations. The track and vehicle properties are detailed below.

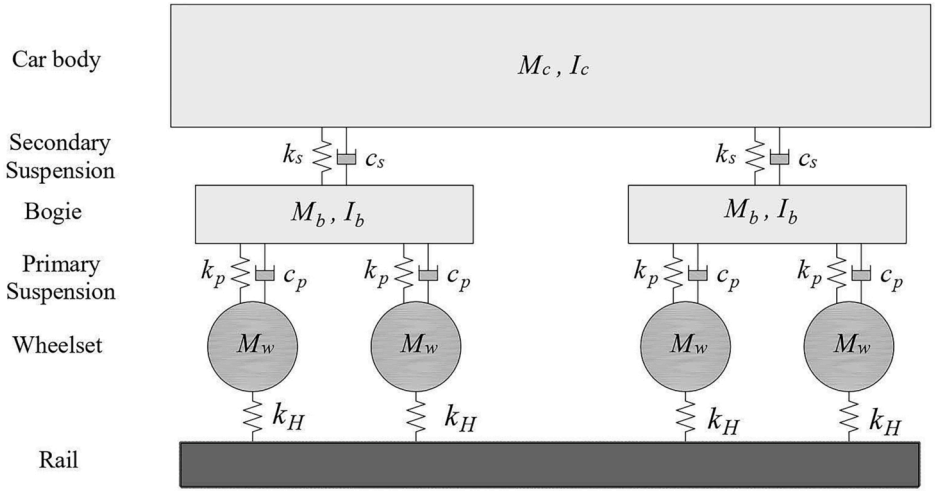

Fig. 6. Schematic of full vehicle model.

3.1. Track geometries and properties

The mesh of the track-soil-bridge structure uses a constant element size of 0.2 m (equal to the width of each sleeper) in the X direction. The maximum element size in the Y and Z directions is 0.3 m and 0.2 m, respectively.

To perform the moving vehicle simulation and capture the dynamic behaviour of the track structure and embankment, a total model length of 80 m in the X axis is used. This model length consists of 60 m for the embankment and 20 m for the bridge. As a result, the total number of meshing elements is 289,441. The track structure is a plain line with a standard gauge of 1.435 m. The spacing between each sleeper is 0.6 m, and the length of the bridge abutment is 3 m. The geometries for each track component in the Y and Z axes are given in Table 2.

For the earthwork application, the UGM (softer material) and CBM (stiffer material) are selected based on published literature [34]. Fig. 7 presents the geometries of the earthwork configurations used:

a) **Single trapezoid**: consists of UGM material with a trapezoid shape that is 20 m in length on the X-axis and has a slope of 3:2 (horizontal: vertical). The region between 20 m and 23.6 m is considered to capture the impact of a single trapezoid and an inverted trapezoid. The 23.6 m length represents the exit of the embankment-bridge transition.

b) **Double trapezoid**: consists of two sections of UGM and CBM. The 3 m trapezoid of CBM with a slope of 1:1 is located next to the transition zone entry. The UGM section is built with a trapezoidal shape that is 17 m in length and has a slope of 3:2. The region between 0 m (transition zone entry) and 5.4 m is significant for capturing the responses due to the double trapezoid.

c) **Single trapezoid (inverted):** consists of an inverted trapezoid of UGM at the transition zone exit (23.6 m). The dimension and slope remain the same as those of a single trapezoid.

d) **Double trapezoid (inverted):** consists of an inverted trapezoid of UGM at the transition zone exit (23.6 m) and a 3 m trapezoid of CBM with a slope of 1:1 next to the transition zone entry. The detailed dimensions and slope are similar to those of a double trapezoid.

Then, the values of material parameters for each track component are selected based on similar studies [34–36,54] as summarised in Table 3.

Regarding Table 3, the rail properties are UIC60. To account for rail pad stiffness in solid element modelling, an equivalent modulus of 7.91 MPa is used, based on a pad stiffness of 255 kN/mm, considering the actual pad geometry and Poisson's ratio effect [57]. The Rayleigh damping coefficients of the railpad are $\alpha = 5\ s^{-1}$ and $\beta = 3.75E\text{-}02$ s (approximated as 22.5 Ns^2/m of viscous damping). For the remaining components, $\alpha = 4.80\ s^{-1}$ and $\beta = 1.52E\text{-}04$ s, based on a damping ratio of 3%.

Table 2
Geometrical dimension of model components.

Component	Height (m) in Y-axis	Full Width (m) in Z-axis
Rail	0.218	0.035
Rail pad	0.008	0.035
Sleeper	0.24	2.6
Ballast	0.36	5.90
Sub-ballast	0.12	7.00
Concrete Slab	0.36	5.90
HBL	0.24	5.90
FPL	0.12	7.00
Subbase	0.36	7.00
Embankment	2.4	9.00
Bridge Abutment	2.4	9.00
Bridge deck	0.36	7.00

3.2. Vehicle properties

The rolling stock properties are based on the Alfa Pendular high-speed train, as shown in Table 4.

3.3. Loading configurations

A sensitivity analysis is performed to gain insights into the effect of combined earthwork solutions and track form permutations on transition zone dynamics. The study also considers the influence of soil stiffness improvement and train speed.

Stationary rail receptance tests and moving load simulations are performed to study dynamic behaviour. In the receptance tests, a vertical Heaviside unit force is applied at the railhead and the deflection at the same location is recorded. The test is conducted at different locations, as shown in Fig. 8. Peaks correspond to the natural frequencies of individual track-ground components, and the sharpness of these peak magnitudes is related to component damping.

For the moving load simulations, the vehicle moves in the direction from the embankment to the bridge. The study investigates and presents the time domain results of vertical rail displacement (maximum) and deviator stress distribution in the longitudinal direction. The rail displacement is captured at the top node of the rail (Location U1), and the deviator stress is measured at the top of the subbase (Location S1), as shown in Fig. 9.

The performance of the earthwork solutions is evaluated by investigating the change in response of receptance, displacement and stress distribution after reinforcement. Lower magnitudes of receptance

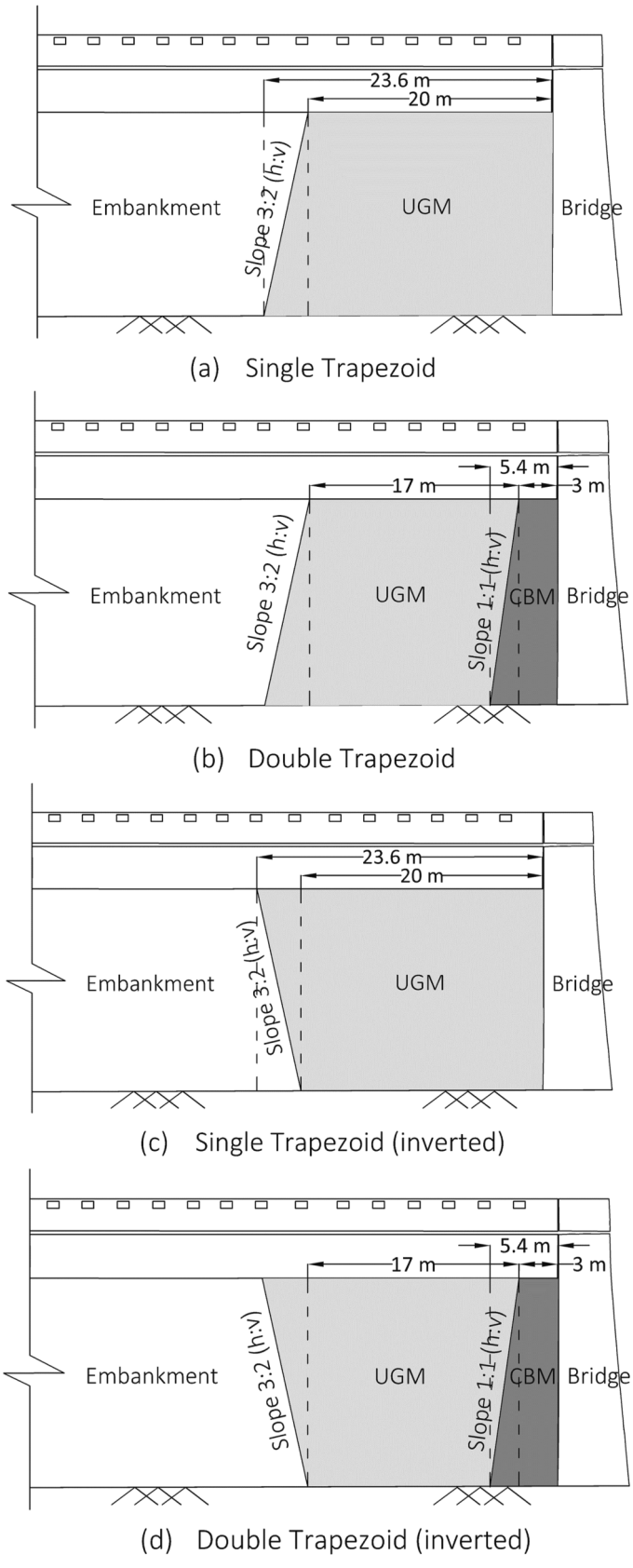

Fig. 7. Earthwork designs.

Table 3
Material properties used in the numerical model.

Component	Density (ρ) Unit: kg/m^3	Young modulus (E) Unit: MPa	Poisson Ratio (ν)
Rail	7850	210,000	0.300
Rail pad	1000	7.91	0.491
Sleeper/ Concrete slab	2500	30,000	0.200
Ballast	1600	200	0.120
Sub-Ballast	2000	150	0.300
HBL	2200	10,000	0.100
FPL	1900	110	0.200
Subbase/ Embankment	2000	120	0.350
UGM	2000	400	0.300
CBM	2200	8,000	0.300
Abutment/Bridge deck	2500	33,000	0.200

Table 4
Alfa Pendular parameters.

Parameter	Value
Axle spacing (m)	2.9
Bogie spacing (m)	19
Car body mass (kg)	329x10^2
Car body pitching moment of inertia (kg m^2)	208x10^2
Bogie mass (kg)	4932
Wheelset mass (kg)	1538
Bogie pitching moment of inertia (kg.m2)	5150
Primary suspension stiffness (kN/m)	3420
Primary suspension viscous damping (Ns/m)	360x10^2
Secondary suspension stiffness (kN/m)	1320
Secondary suspension viscous damping (Ns/m)	360x10^2

indicates a stiffer structural response.

4. Results and analysis

The analysis consists of five sections. After defining the frequency range of interest, results are presented related to the track structure type, earthwork configuration, earthwork stiffness and train speed.

4.1. Frequency range of interest

The first investigation aims to determine the general dynamic characteristics of embankment-bridge transition zones and identify the frequency range of interest. To achieve this, receptance tests are performed on both sides of the transition (Locations R1, R2, R3 and R5 in Fig. 8). Fig. 10 presents the rail receptance response for the ballasted and slab tracks spanning the embankment-bridge structure. Considering the curve magnitudes, the response of the ballasted track is significantly greater than that of the slab for all testing locations, due to the ballasted track having a lower bending stiffness than the slab.

Further, the peak response at the bridge is higher than that at the embankment and occurs at a higher frequency (exceeding 200 Hz) than the embankment side (between 0 and 100 Hz) for both ballasted and slab tracks. It also has a more pronounced peak. This is because the concrete bridge is stiffer than the embankment and has lower damping. However, considering the main focus of this work is on earthwork solutions for transition zones, it is seen that the main frequency range of interest is between 0 and 100 Hz. Therefore, for the remainder of the work, this range is focused upon.

4.2. The effect of track structure types

First, the receptance characteristics of the two track structures are investigated. Receptance is performed on the embankment 10 m from the bridge (location 3 in Fig. 8). Fig. 11 shows the ballasted track receptance has a greater magnitude than the slab, indicating it is less stiff. However, the dominant peak for both tracks is similar, lying at approximately 20 Hz. On the same figure, the excitations after reinforcing the embankment are compared for both ballasted and slab tracks. It is seen that the dominant peak at approximately 20 Hz is reduced, and the energy at approximately 75 Hz is either increased or introduced. This is true for both track structures and indicates a spreading of the dynamic energy over a wider frequency range, thus

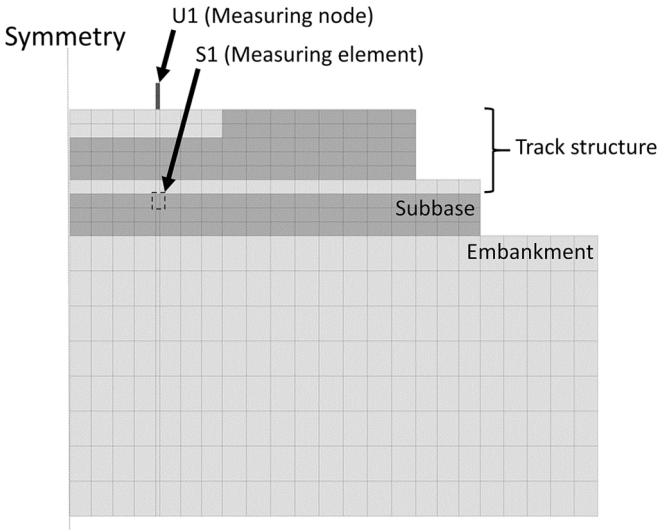

Fig. 9. Measuring locations for rail displacement and subbase stress.

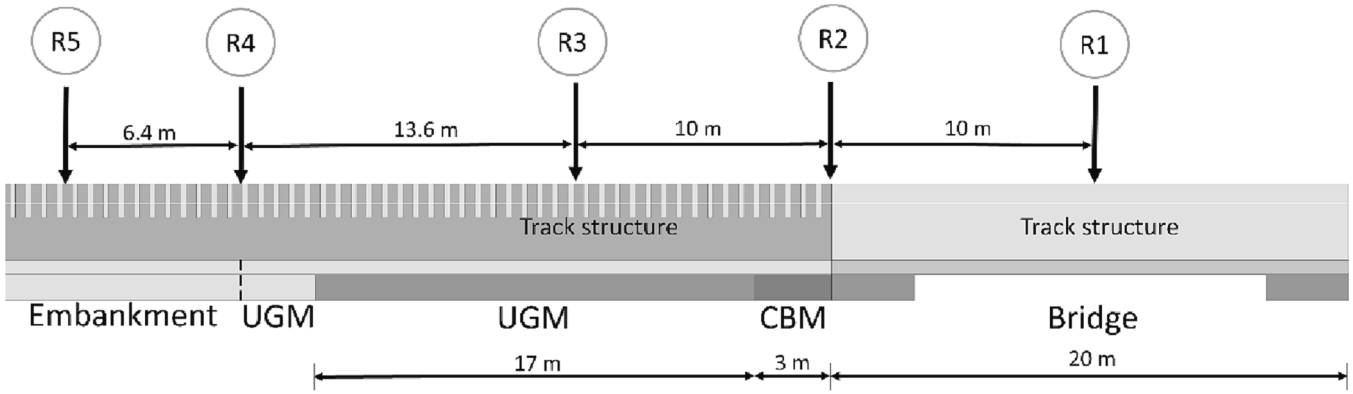

Fig. 8. Rail receptance test locations.

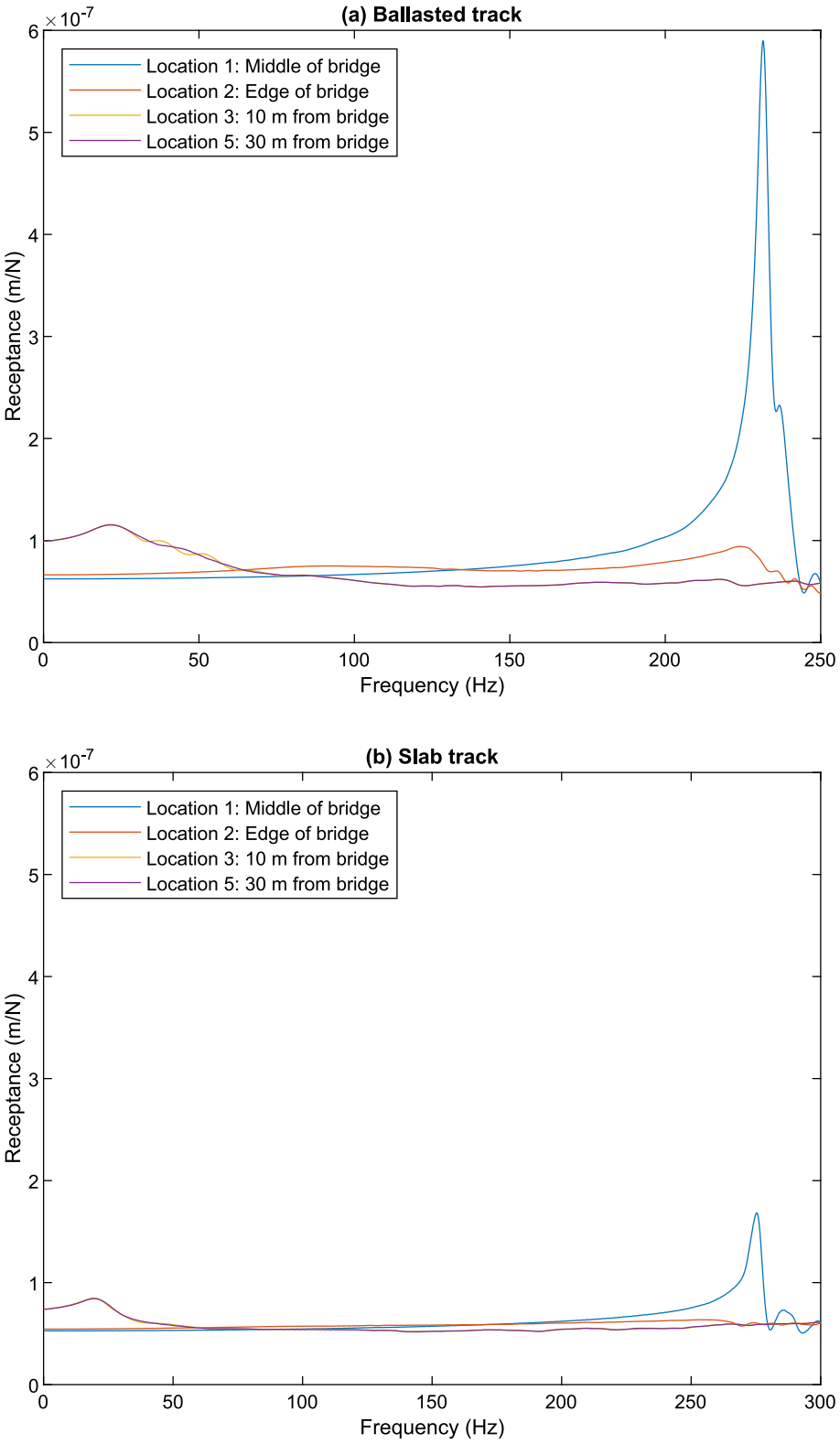

Fig. 10. Rail receptance at different locations of embankment-bridge transition, (a) Ballasted track, (b) Slab track.

possibly improving dynamic performance.

To investigate this further, the response of the track due to moving loads is considered. Fig. 12 presents the time-domain results of vertical rail displacement with and without the earthwork stiffening for the three track-form combinations: a) ballasted track on both structures, b) ballasted track on the embankment and slab track on the bridge, and c) slab track on both structures. Comparing the displacement on both sides of the transition, the deflection is larger on the embankment due to its reduced stiffness. This is true for all track forms; however, the difference is greatest when the track on the earthworks is ballasted.

The UGM earthwork solution is seen to decrease the differential displacement across the transition. This is true for all the tracks and

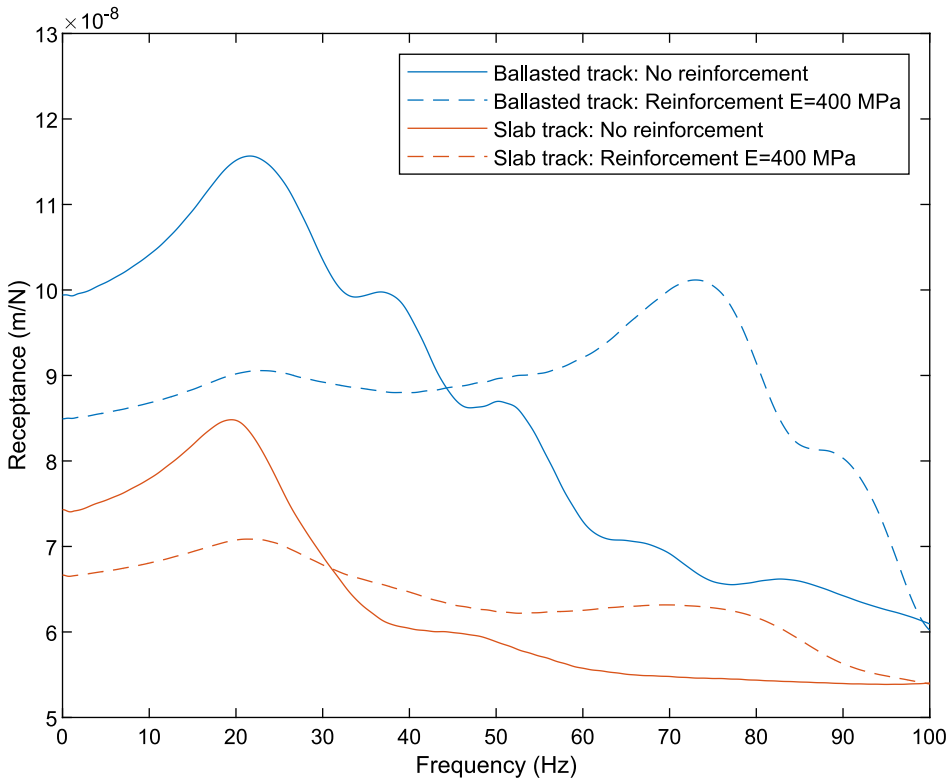

Fig. 11. Rail receptance before and after applying earthwork solution.

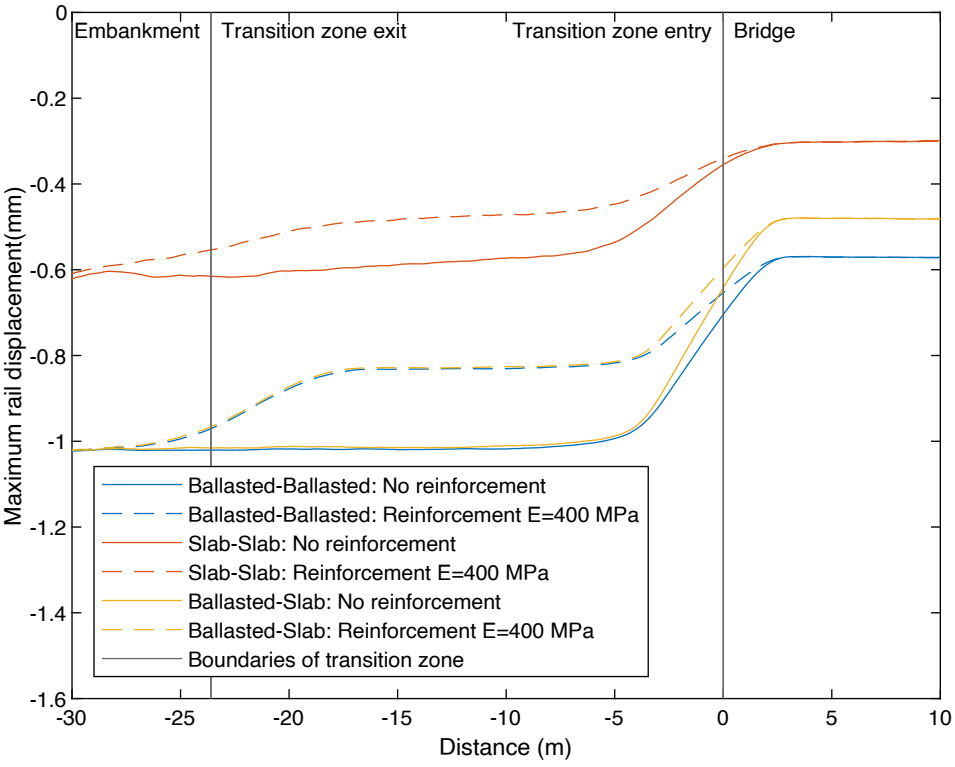

Fig. 12. Rail displacement for different track permutations.

results in two smaller sub-transitions rather than a single larger one. The performance is particularly strong for the slab->slab track configuration, where the displacement change is relatively gradual along the entire transition zone length.

Regarding stress distribution, Fig. 13 presents the deviator stress distribution for ballasted and slab tracks. It is seen that the use of UGM for reinforcing the earthwork solution can reduce the stress for both track types. The reduction is more significant in the ballasted track

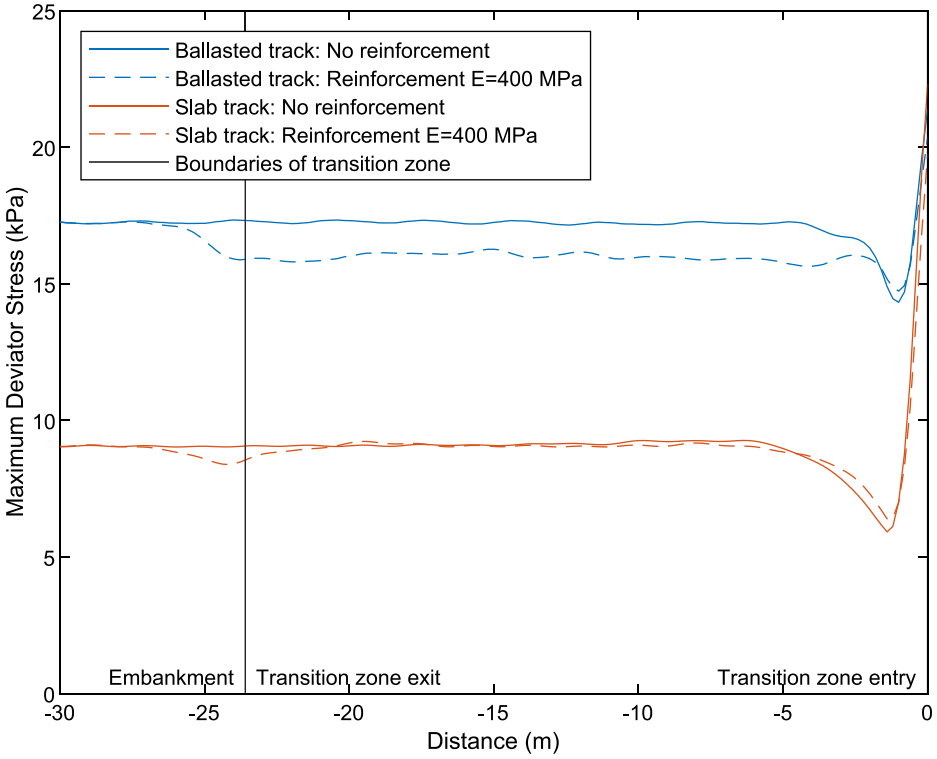

Fig. 13. Subbase deviator stress before and after applying earthwork remediation.

compared to the slab track, consistent with the displacement analysis. The maximum stress occurs at the transition zone entry (X = 0) for both types of tracks due to a sudden change in track stiffness, from low stiffness at the embankment to high stiffness on the bridge. A single layer of UGM (E = 400 MPa) improves the subbase stress up to approximately 3 m from the bridge.

4.3. *The effect of earthwork configurations*

This section examines the impact of four different earthwork

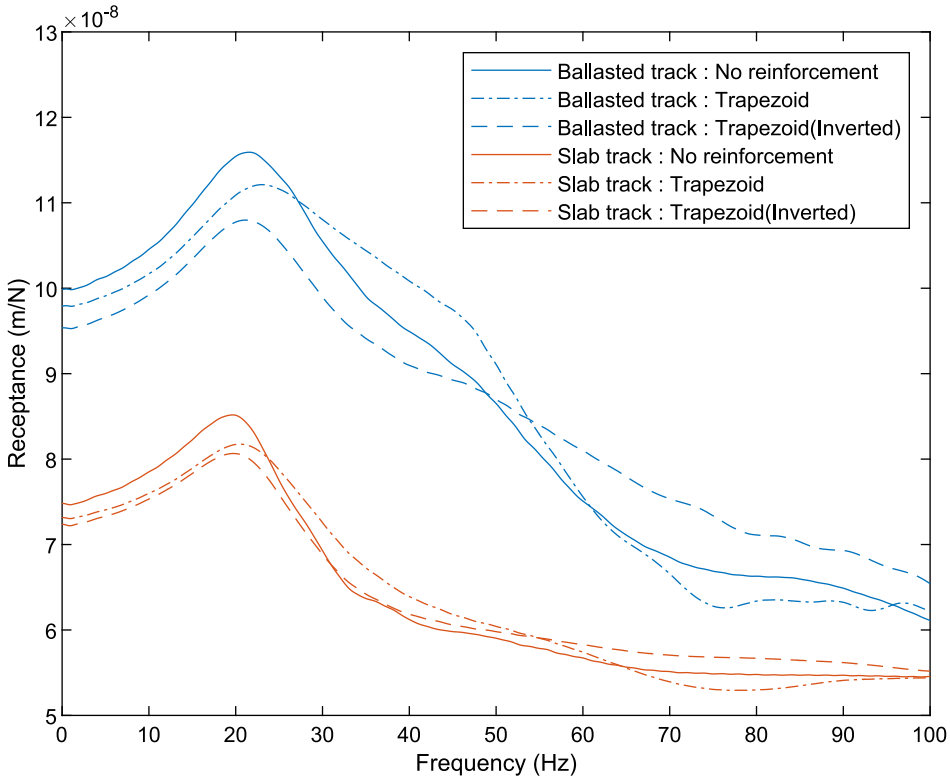

Fig. 14. Rail receptance for different earthwork configurations.

configurations on the response of ballasted and slab tracks: single and double trapezoid shapes, and single and double inverted trapezoid shapes.

Firstly, the receptance of ballasted and slab tracks on the embankment at the transition zone exit (location 4 in Fig. 8) is discussed. Fig. 14 presents the receptance response for various earthwork shapes. The results demonstrate using the inverted trapezoid earthwork for both ballasted and slab tracks results in a lower magnitude at the 20 Hz peak compared to the other configurations. However, it shows an increased response after approximately 50 Hz.

4.3.1. Reinforcement of the ballasted support for differing earthwork configurations

In addition to the receptance results, Fig. 15 and Fig. 16 show the rail displacements induced by train passage for the ballasted->ballasted track and ballasted->slab track. When comparing the impact of the single trapezoidal earthwork solution versus the single inverted trapezoid, both track types exhibit similar displacement performance. In terms of the effect of the double trapezoid configurations, they are found to help smooth the displacement change in the regions close to the bridge deck (-10 m to 3 m).

Fig. 17 presents the stress distribution for the ballasted track, considering only the embankment. Similar to the displacement response, the results indicate the inverted trapezoid shape is more effective in reducing stress at the transition zone exit region than a trapezoid shape. Additionally, a double configuration is found to be more efficient in reducing stress at the entry region than a single configuration. This leads to a reduction in the stress peak at the transition zone entry (X = 0).

4.3.2. Reinforcement of the slab track support for differing earthwork configurations

The rail displacement and stress distribution results for the slab->slab track are presented in Fig. 18 and Fig. 19 respectively. The findings suggest there is no significant difference in displacement or stress reduction between a trapezoidal or inverted trapezoidal earthwork solution. However, it is found that the use of double configuration can help smooth the displacement response at the locations near the transition zone entry.

4.4. The effect of earthwork stiffness

Previous studies (i.e., Table 1) have suggested the use of varying earthwork improvement solutions to optimise transition zone performance. However, due to the varying track properties and geometries in each study, it is challenging to compare dynamic track performance across each. To address this issue, this section is divided into two parts based on track type: ballasted and slab track. Four stiffness values, namely, 120 MPa (an embankment constructed mainly from lower-quality granular material), 200 MPa (UGM with graded gravel), 400 MPa (UGM with graded gravel and 3% cement), and 600 MPa (UGM with graded gravel and 5% cement), are selected based on [33]. The remaining properties, including density, Poisson's ratio, and damping, remain constant, as shown in Table 3.

4.4.1. Reinforcement of the ballasted track support for differing earthwork stiffnesses

In the receptance test, measurements are taken 10 m from the bridge edge (location 3 in Fig. 8). Fig. 20 presents the receptance results for different material stiffnesses for the ballasted track. All earthwork solutions show reduced deflection at low frequencies (0–50 Hz) as the reinforcement stiffness increases. However, as the reinforcement stiffness increases, an additional peak amplitude appears between 70 and 90 Hz, and its magnitude also increases. This is because increasing the stiffness of the reinforcement shifts the excitation energy to be more confined within the upper track layers rather than the lower layers.

Moving load simulations are then performed using four material stiffness' (120, 200, 400 and 600 MPa) considering both ballasted->ballasted and ballasted->slab track configurations. Fig. 21 and Fig. 22 present the rail displacement histories for both track types, while Fig. 23 shows the stresses. In the case of no reinforcement, there is no change when moving from the embankment into the transition zone because the material properties are constant. However, there is a large change when moving onto the bridge. In contrast, each of the cases with

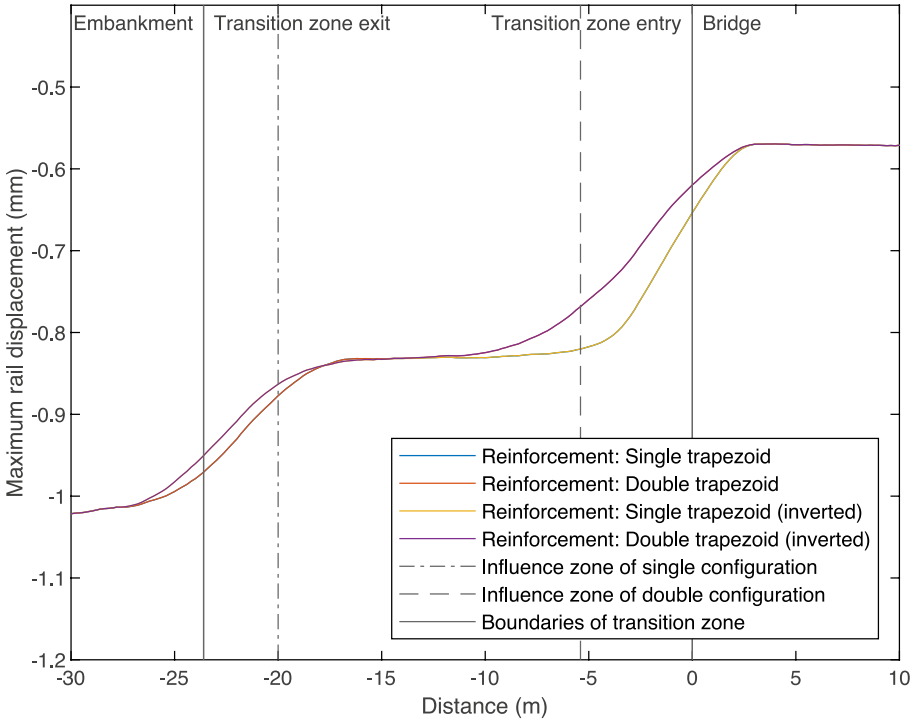

Fig. 15. Rail displacement for different earthwork configurations supporting the ballasted-ballasted track.

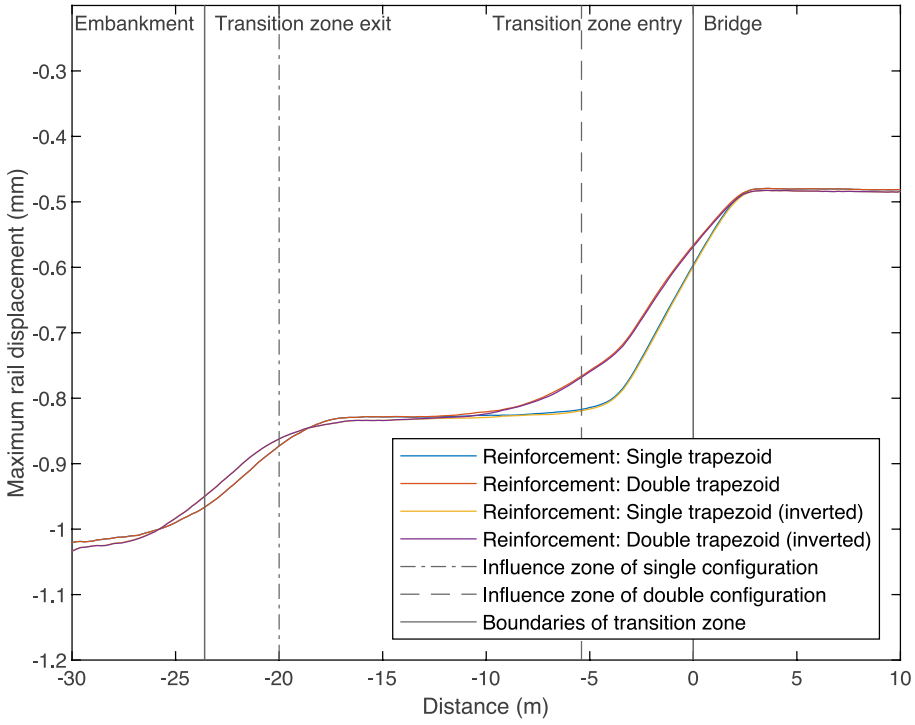

Fig. 16. Rail displacement for different earthwork configurations supporting the ballasted-slab track.

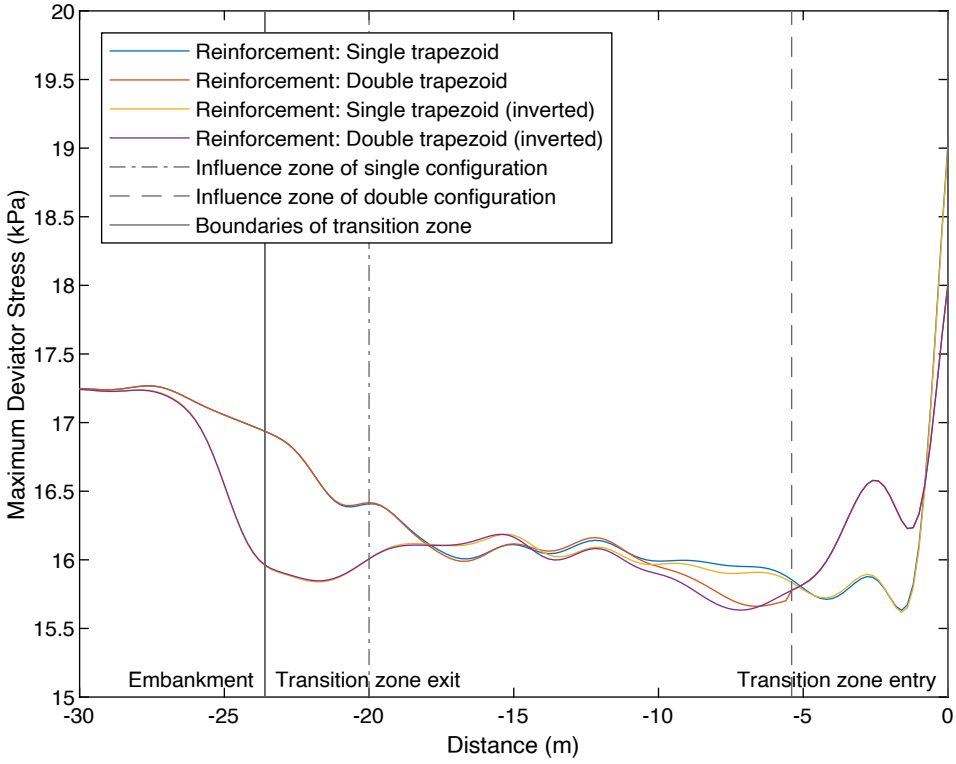

Fig. 17. Subbase deviator stress for different earthwork configurations supporting the ballasted track.

reinforcement shows a marked change in deflection when entering and exiting the transition zone. The lower reinforcement stiffness values (e.g., 200 MPa) show a small change when moving from the embankment and a large change when moving onto the bridge. However, the 600 MPa case shows an approximately equal split in the displacement change at both locations. Therefore, this solution is likely to result in reduced settlement at both 'mini-transition' locations. This is likely to be a more optimum solution compared to the non-reinforced option, which will have high localized settlement at the bridge-embankment interface.

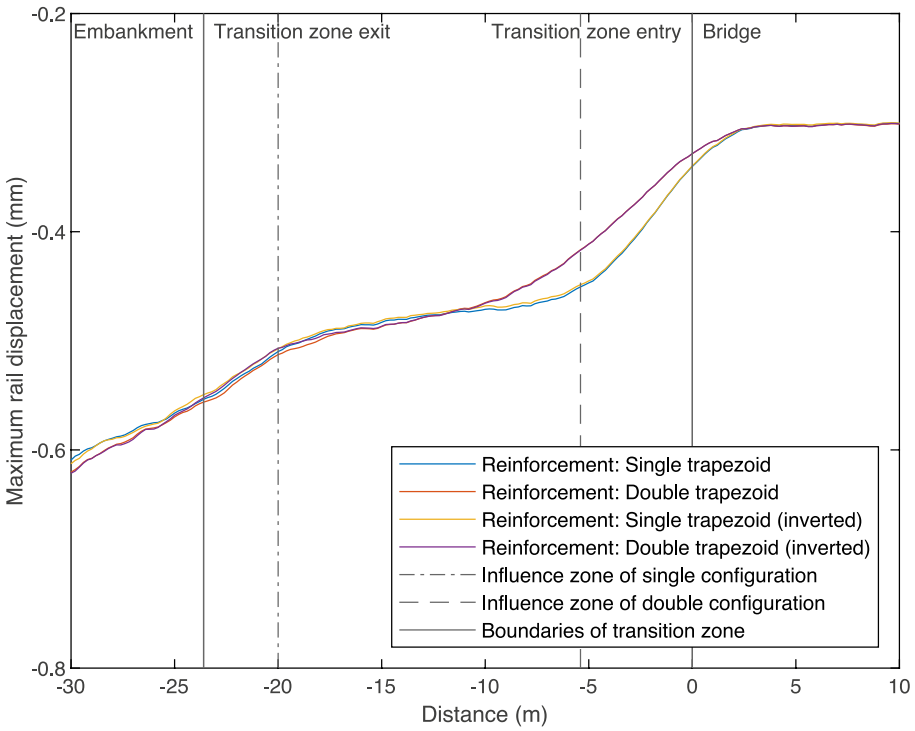

Fig. 18. Rail displacement for different earthwork configurations supporting the slab-slab track.

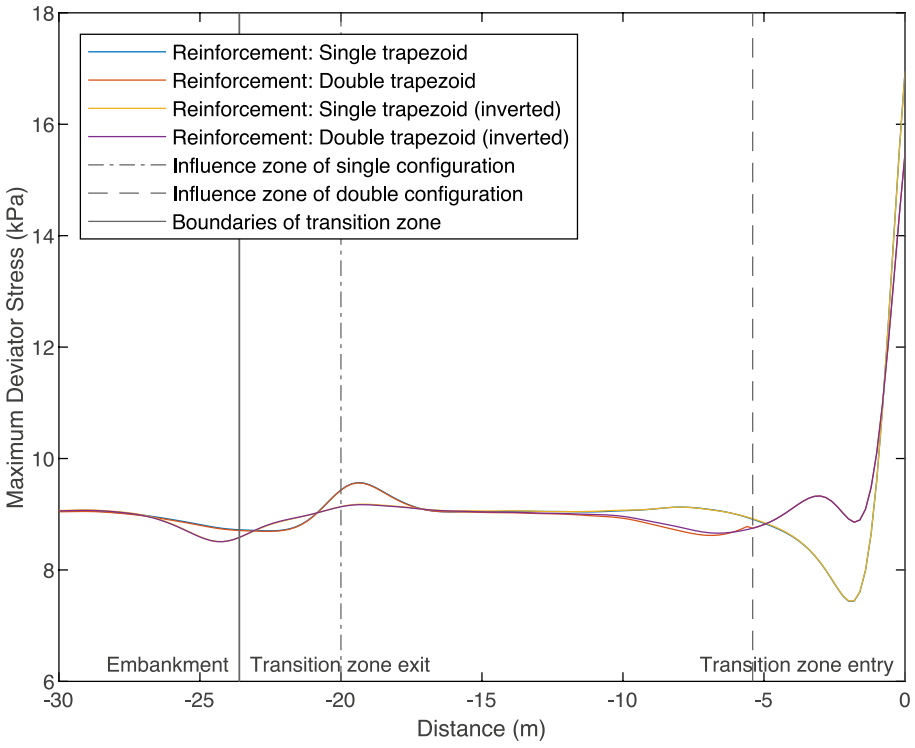

Fig. 19. Subbase deviator stress for different earthwork configurations supporting the slab track.

4.4.2. Reinforcement of the slab track support for differing earthwork stiffnesses

The receptance test was also performed on the slab track at the same testing location. Fig. 24 shows the receptance results for different material stiffnesses supporting the slab track. The findings indicate the higher ground material stiffness leads to a reduced receptance magnitude in the 0–50 Hz range, which is similar to the results observed for the ballasted track. Similarly, there is an increase in energy in the 50–100 Hz range, although it is less pronounced with the peaks either similar or lower than those in the 0–50 Hz range.

Regarding rail displacement histories, Fig. 25 shows using higher-stiffness materials results in a smoother displacement profile along the transition. This finding is similar to that for the ballasted track, with the highest stiffness showing best performance and two smaller transition

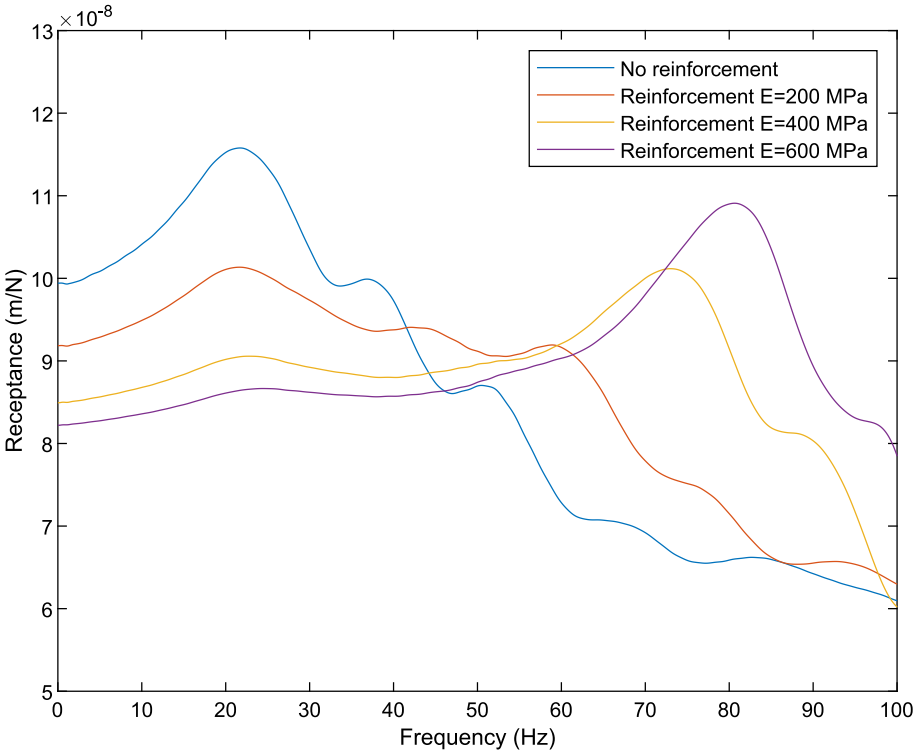

Fig. 20. Rail receptance for different reinforcement stiffnesses supporting the ballasted track.

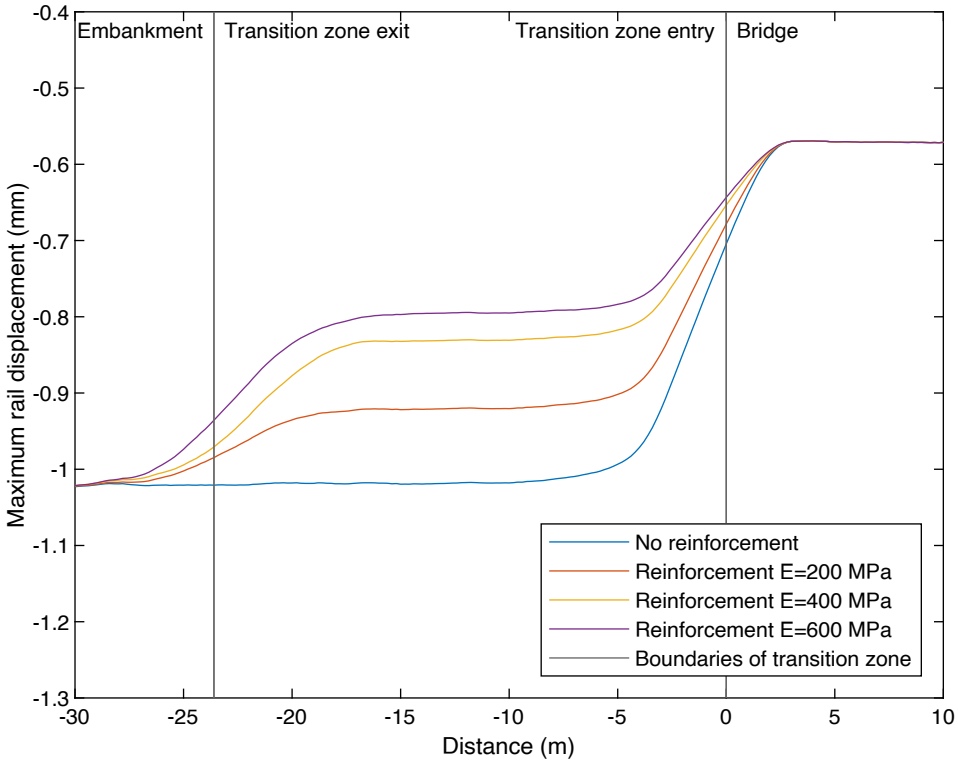

Fig. 21. Rail displacement for different reinforcement stiffnesses supporting the ballasted-ballasted track.

zones being created. It is also noticeable that the benefit is not linear, as changing from 0 to 200 MPa provides a greater benefit compared to changing from 400 to 600 MPa. The stress results are shown in Fig. 26, where the benefit is marginal.

4.5. The influence of train speed

This section investigates the dynamic behaviour of the transition zone with earthwork reinforcement using the benchmark case, which involves a single trapezoidal shape of UGM material, for three different

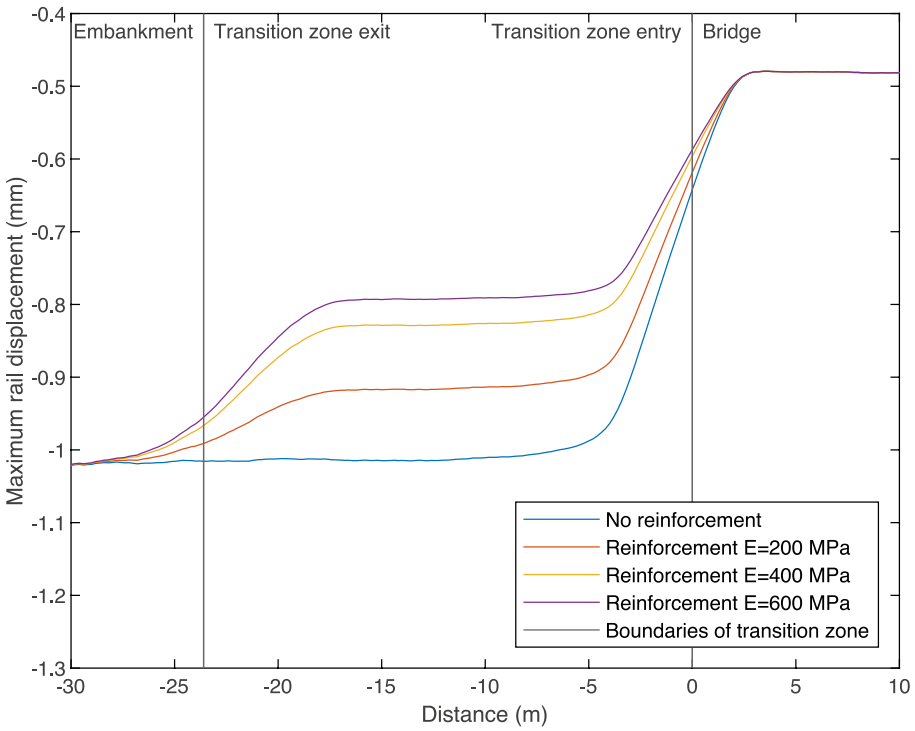

Fig. 22. Displacement for different reinforcement stiffnesses supporting the ballasted-slab track.

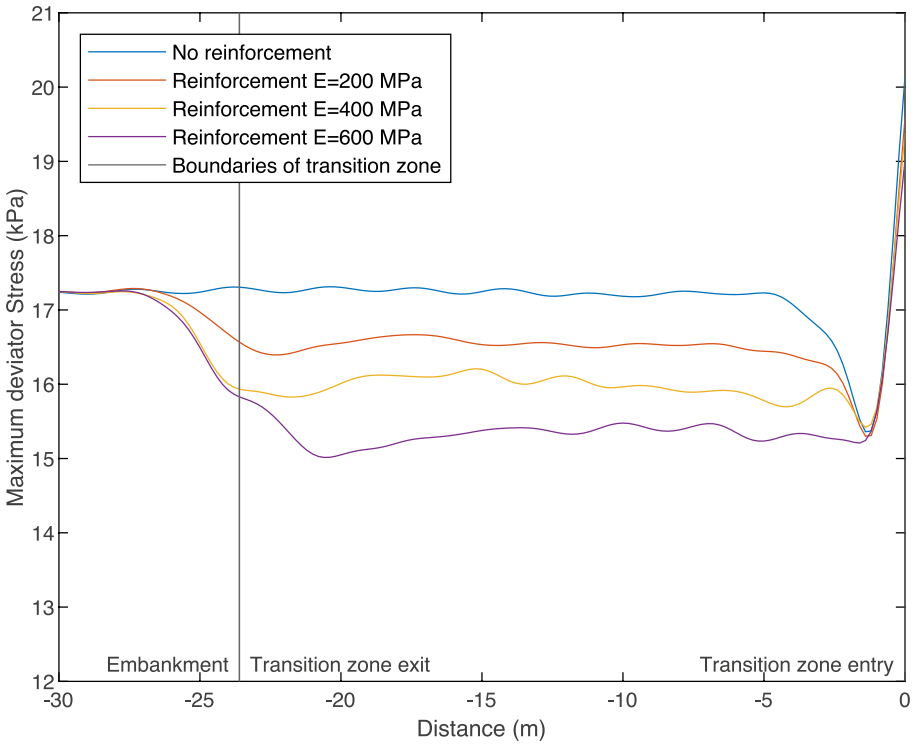

Fig. 23. Subbase deviator stress for different reinforcement stiffnesses supporting the ballasted track.

train speeds. To achieve this, simulations are performed for two additional train speeds of 150 and 250 km/hr, and the results are compared with the original speed of 212 km/hr. Since the unreinforced embankment stiffness is 120 MPa, all train speeds are below the track-ground critical speed. The investigation is divided into two sections based on the track forms: ballasted and slab track.

4.5.1. *Reinforcement of ballasted track support considering train speed*

Fig. 27 and Fig. 28 present the rail displacement results versus train speed for ballasted->ballasted and ballasted->slab tracks, respectively. Higher train speeds result in greater rail displacement on the earthworks, especially on the unreinforced embankment. However, the impact on the transition zone and the bridge is minimal, which is true for both ballast and slab tracks. Regarding stress, Fig. 29 shows a significant

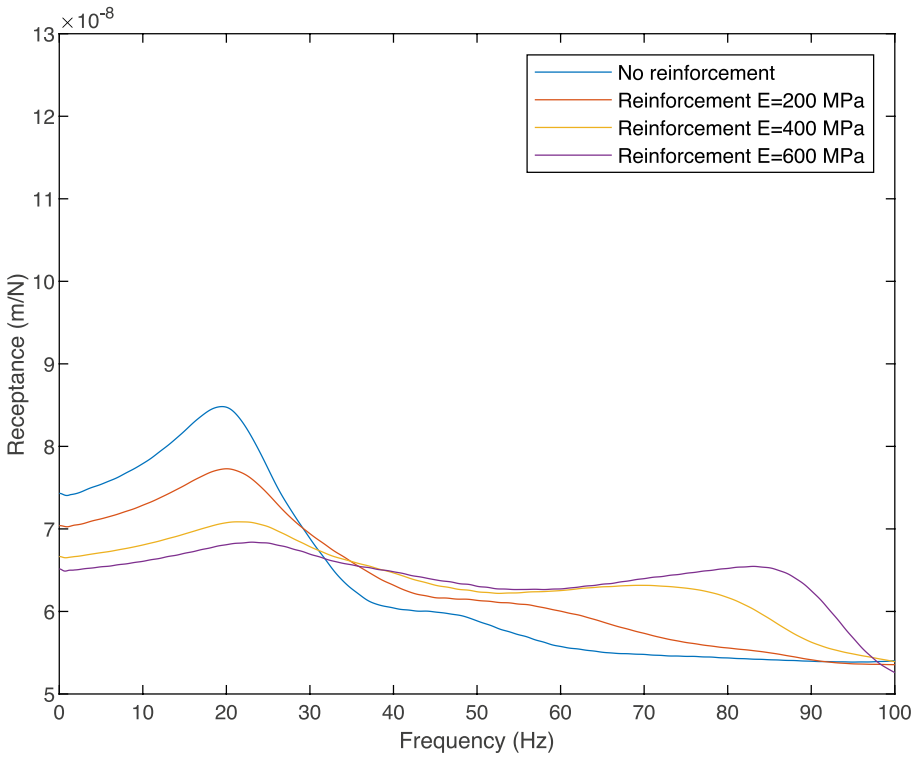

Fig. 24. Rail receptance for different reinforcement stiffnesses supporting the slab track.

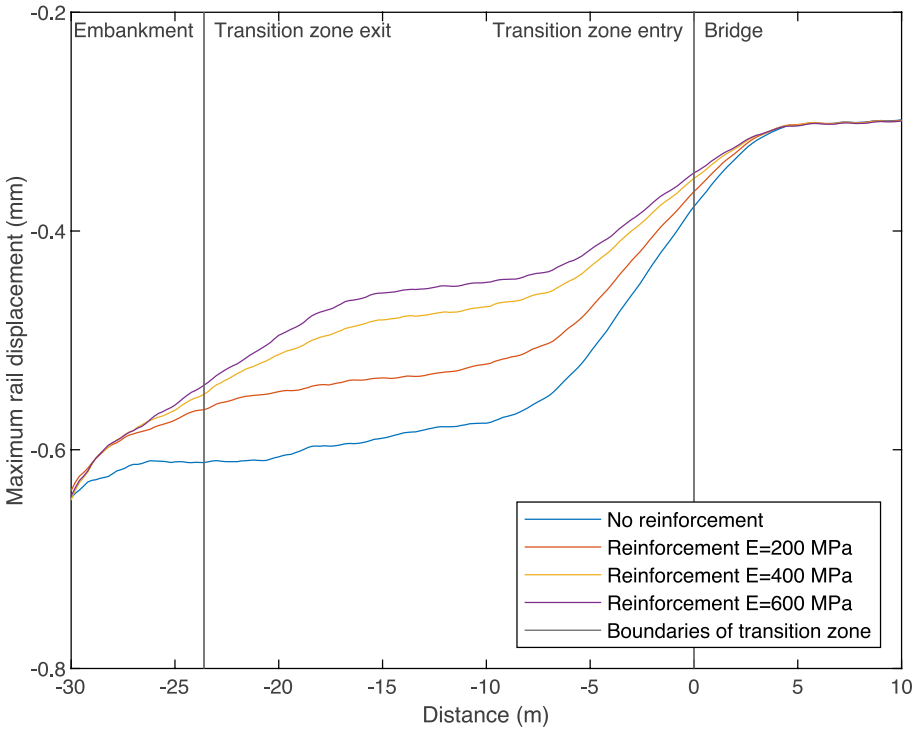

Fig. 25. Rail displacement for different reinforcement stiffnesses supporting the slab-slab track.

increase in stress with increasing train speed.

4.5.2. Reinforcement of slab track support considering train speed

Fig. 30 and Fig. 31 show the rail displacement and stress distribution, respectively, for the slab->slab track configurations. Increasing the train speed on slab tracks has a lower impact on displacement compared to ballasted track. Regarding stress, similar to the ballasted track, the relationship with speed is more apparent, with higher speeds inducing greater stresses. This is consistent with [45].

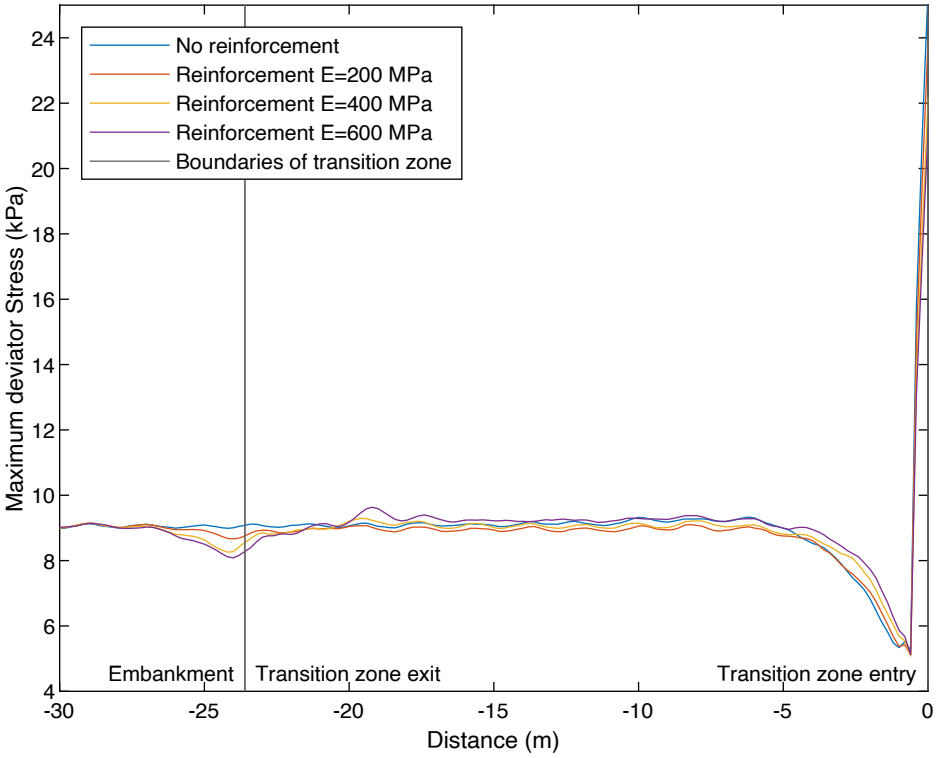

Fig. 26. Subbase deviator stress for different reinforcement stiffnesses supporting the slab track.

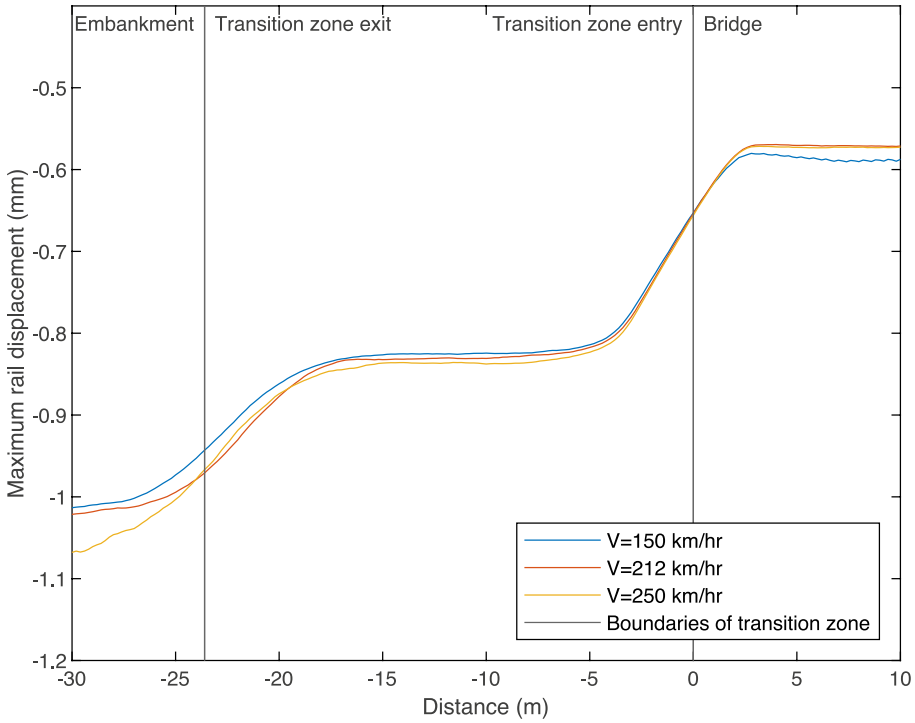

Fig. 27. Rail displacement for different train speeds on the ballasted-ballasted track.

5. Discussion

This work investigates a range of geometries for transition zone ground improvement, and the effect of train speed on each. Although some of the more complex geometries are shown to potentially offer performance benefits it is important to also consider the practical constraints related to designing these for construction. In particular, the construction of earthworks to exact geometries, thicknesses, compaction levels and stiffness values is challenging and may not be achievable or practical. Further, it may increase the cost compared to a simpler earthwork solution yet deliver marginal performance. Therefore, a range of issues must be considered before choosing a design solution. To

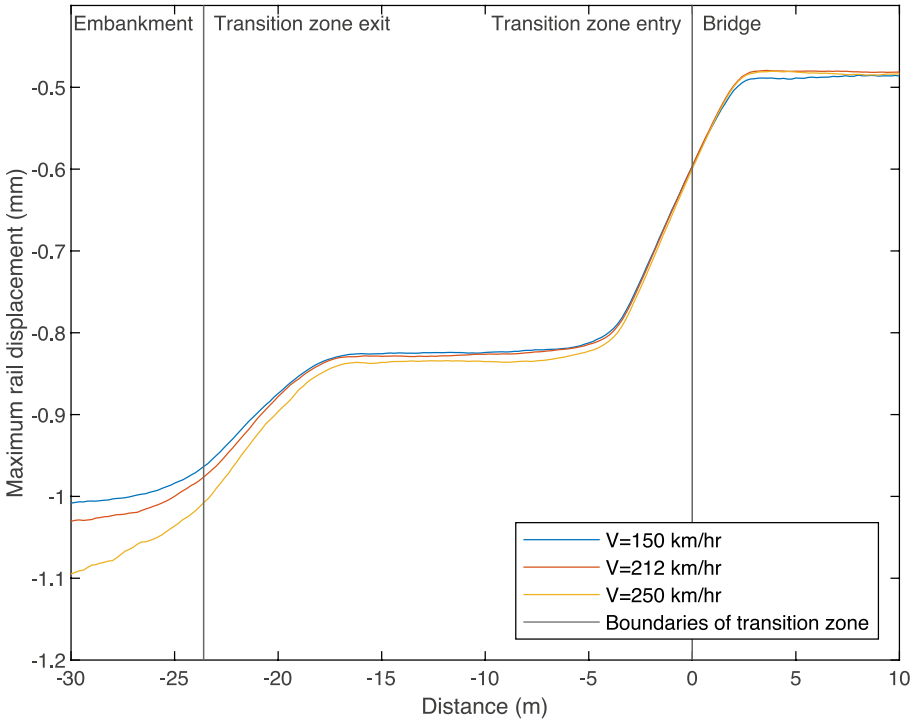

Fig. 28. Rail displacement for different train speeds on the ballasted-slab track.

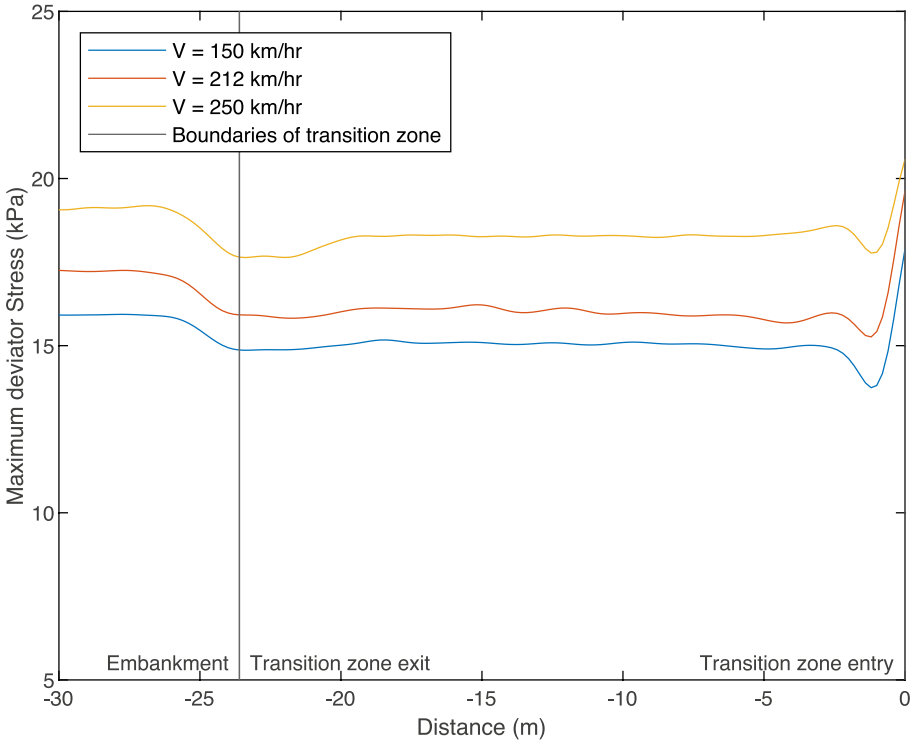

Fig. 29. Subbase deviator stress for different train speeds on the ballasted track.

help compare a wider range of solutions and the impact of a wider range of variables on the overall design choice, optimisation techniques may prove helpful [61]. For example, using an optimisation algorithm for transition zone design [40], earthwork properties [62], operations [63] and economic and environmental impact [64].

6. Conclusions

This paper presents a numerical analysis of the dynamic track behaviour at embankment-bridge transition zones using a 3D finite element model. The model consists of a track transition over an earthwork-bridge support, with the moving load implemented using a rigid multi-body system and a Hertzian spring. It considers differing

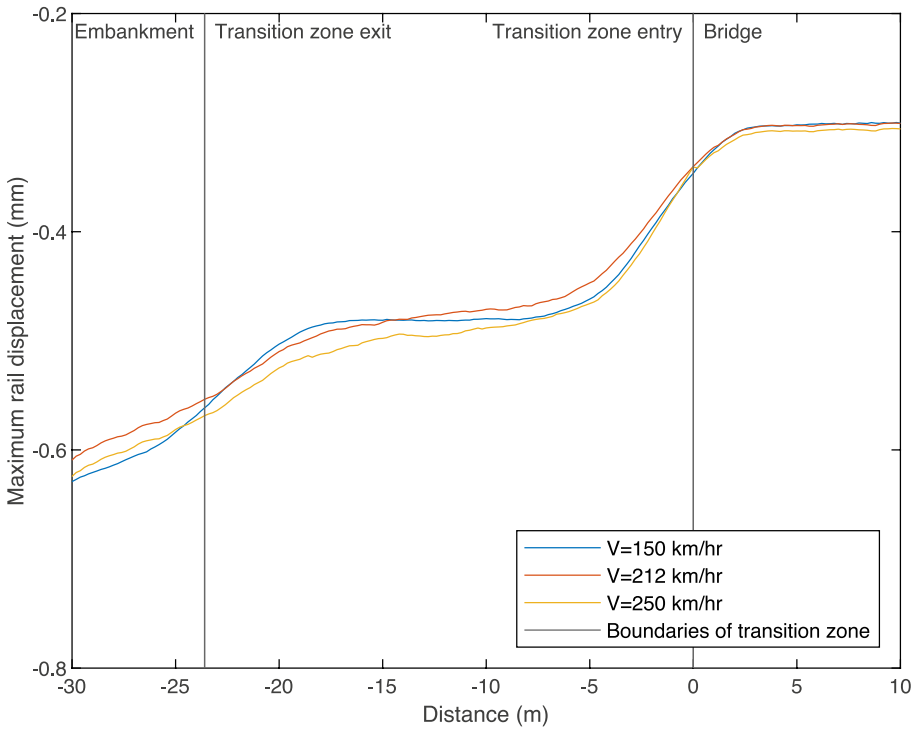

Fig. 30. Rail displacement for different train speeds on the slab-slab track.

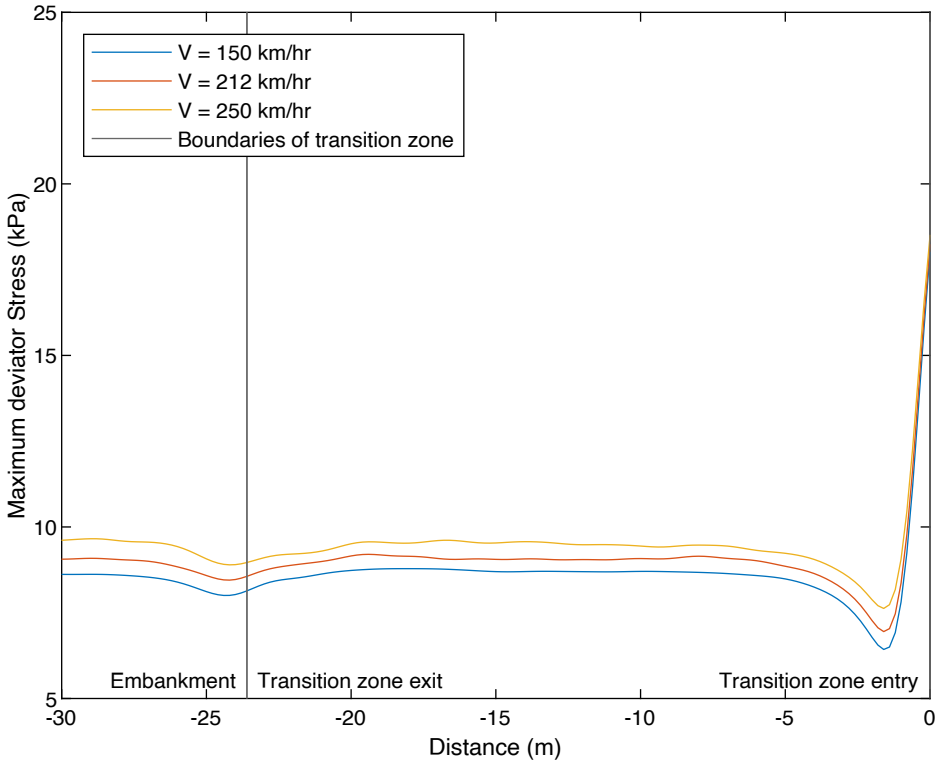

Fig. 31. Subbase deviator stress for different train speeds on the slab track.

earthwork material stiffnesses and geometry configurations, subject to varying train speeds over differing track structures (ballasted and concrete slab). The conclusions are:

- Using earthwork solutions can improve the dynamic characteristics of the track, including rail displacement and deviator stress distribution in the subbase across the embankment-bridge transition zone for all track types. The benefits are greater for ballasted tracks than slab tracks due to their lower bending stiffness.
- Special attention can be given to the first 3 m from the transition zone entry (adjacent to the bridge) to minimise dynamic effects. For

example, the use of additional reinforcement of high-stiffness material can create a 'double' trapezoid configuration.
- A 'double' trapezoid configuration has the potential to improve track dynamics by creating two smaller transition zones rather than one larger one. The stiffness profile along the track can be optimised to balance the dynamic changes across each mini transition.
- For the cases considered, a material stiffness of 400 MPa was sufficient to reinforce the earthworks for both ballasted and slab track.
- Higher train speeds induce greater increases in ballasted tracks compared to slabs. There is a clear relationship between speed and induced stress, which is an influencing factor in track settlement.
- Although arbitrary earthwork profiles can be analysed using numerical tools, the physical construction of complex geometries on-site can be challenging. Therefore, any potential benefits should be weighed against constructability considerations.

CRediT authorship contribution statement

P. Chumyen: Formal analysis, Methodology, Software, Writing – original draft. **D.P. Connolly:** Conceptualization, Methodology, Resources, Supervision. **P.K. Woodward:** Writing – review & editing. **V. Markine:** Supervision, Writing – review & editing.

Declaration of Competing Interest

The authors declare that they have no known competing financial interests or personal relationships that could have appeared to influence the work reported in this paper.

Data availability

Data will be made available on request.

Acknowledgements

Leverhulme Trust (UK -PLP-2016-270), University of Leeds, Delft University of Technology, IN2ZONE (European Commission GA: 101014571)

References

[1] D. Kite, G. Siino, M. Audley, Detecting embankment instability using measurable track geometry data, Infrastructure 5 (29) (2020) pp.
[2] C. Charoenwong, D.P. Connolly, P.K. Woodward, P. Galvín, P. Alves Costa, Analytical forecasting of long-term railway track settlement, Comput. Geotech. 143 (2022) 104601.
[3] A. Ramos, A. Gomes Correia, R. Calçada, D.P. Connolly, Ballastless railway track transition zones: an embankment to tunnel analysis, Transp. Geotech. 33 (2022) 100728.
[4] G. Kouroussis, D.P. Connolly, K. Vogiatzis, O. Verlinden, Modelling the environmental effects of railway vibrations from different types of rolling stock: a numerical study, Shock Vib. 2015 (2015) 1–15.
[5] R. Sañudo, L. Dell'Olio, J.A. Casado, I.A. Carrascal, S. Diego, Track transitions in railways: a review, Constr. Build. Mater. 112 (2016) 140–157, https://doi.org/10.1016/j.conbuildmat.2016.02.084.
[6] G. Kouroussis, D.P. Connolly, G. Alexandrou, K. Vogiatzis, Railway ground vibrations induced by wheel and rail singular defects, Veh. Syst. Dyn. 53 (2015), https://doi.org/10.1080/00423114.2015.1062116.
[7] D.P. Connolly, P.A. Costa, Geodynamics of very high-speed transport systems, Soil Dyn. Earthq. Eng. 130 (2020) 105982.
[8] H. Wang, V. Markine, Dynamic behaviour of the track in transitions zones considering the differential settlement, J. Sound Vib. 459 (2019) 114863.
[9] J. E. Nicks, "The bump at the end of the railway bridge," 2009.
[10] D. Li, D. Davis, Transition of Railroad Bridge Approaches, Geotechnical and Geoenvironmental Engineering 131 (11) (2005) 1392–1398, https://doi.org/10.1061/(asce)1090-0241(2005)131:11(1392).
[11] A. Paixão, J.N. Varandas, E. Fortunato, Dynamic behavior in transition zones and long-term railway track performance, Front Built Environ 7 (2021) 1–16, https://doi.org/10.3389/fbuil.2021.658909.
[12] A. Paixão, E. Fortunato, R. Calçada, Design and construction of backfills for railway track transition zones, Proc Inst Mech Eng F J Rail Rapid Transit 229 (1) (2015) 58–70, https://doi.org/10.1177/0954409713499016.
[13] B. Indraratna, M. Babar Sajjad, T. Ngo, A. Gomes Correia, R. Kelly, Improved performance of ballasted tracks at transition zones: a review of experimental and modelling approaches, Transp. Geotech. 21 (2019) 100260.
[14] C. Zhang, et al., Centrifuge modelling of multi-row stabilizing piles reinforced reservoir landslide with different row spacings, Landslides 20 (2023) 559–577.
[15] M. Samadi, N. Jahan, Comparative study on the effect of outrigger on seismic response of tall buildings with braced and RC wall core. I: Optimum level and examining modal response spectrum analysis reliability, Struct. Design Tall Spec. Build. 30 (8) (2021) pp.
[16] N. Jahan, A.M. Heydari Tafreshi, M. Gerami, Assessment of steel structures with a dual system of moment frame with concentrically brace influencing repeated earthquakes, Civil Engineering, Sharif, 2021, pp. 121–132.
[17] P. Hu, C. Zhang, S. Jian, Y. Wang, W. Wang, W. Hui, Dynamic responses of bridge-embankment transitions in high-speed railway: field tests and data analyses, Eng. Struct. 175 (2018) 565–576, https://doi.org/10.1016/j.engstruct.2018.08.079.
[18] G. Lazorenko, A. Kasprzhitskii, Z. Khakiev, V. Yavna, Dynamic behavior and stability of soil foundation in heavy haul railway tracks: a review, Constr. Build. Mater. 205 (2019) 111–136, https://doi.org/10.1016/j.conbuildmat.2019.01.184.
[19] A. Arulrajah, A. Abdullah, M.W. Bo, M. Leong, Geosynthetic applications in high-speed railways: a case study, Proceedings of the Institution of Civil Engineers - Ground Improvement 168 (1) (2015) 3–13.
[20] D.P. Connolly, H.S. Yu, A shakedown limit calculation method for geogrid reinforced soils under moving loads, Geotext. Geomembr. 49 (2021) 688–696, https://doi.org/10.1016/j.geotexmem.2020.11.009.
[21] C. Chen, "Discrete element modelling of geogrid-reinforced railway ballast and track transition zones," 2013.
[22] S. Park, D.S. Kim, U. Kim, S. Jeong, Low compressibility at the transition zone of railway tracks reinforced with cement-treated gravel and a geogrid under construction, Applied Sciences (Switzerland) 12 (17) (2022) pp, https://doi.org/10.3390/app12178861.
[23] P. Punetha, K. Maharjan, S. Nimbalkar, Finite element modeling of the dynamic response of critical zones in a ballasted railway track, Front Built Environ 7 (2021) 1–11, https://doi.org/10.3389/fbuil.2021.660292.
[24] M.L. Palomo, F.R. Barcelo, F.R. Llario, J.R. Herra, Effect of vehicle speed on the dynamics of track transitions, Vibration and Control (2018), https://doi.org/10.1177/1077546317745254.
[25] K. Asghari, S. Sotoudeh, J.-A. Zakeri, Numerical evaluation of approach slab influence on transition zone behavior in high-speed railway track, Transp. Geotech. 28 (2021) 100519.
[26] RhombergSersa, "Keep track: Universal transition module V-TRAS," 2021.
[27] D. M Setiawan, Worldwide hot mix asphalt layer application and scrap rubber and bitumen emulsion studies on railway track-bed, Semesta Teknika 21 (2) (2018), https://doi.org/10.18196/st.212223.
[28] Z. Yu, D.P. Connolly, P.K. Woodward, O. Laghrouche, Settlement behaviour of hybrid asphalt-ballast railway tracks, Constr. Build. Mater. 208 (2019) 808–817, https://doi.org/10.1016/j.conbuildmat.2019.03.047.
[29] A. Sakhare H. Farooq S. Nimbalkar G.R. Dodagoudar Dynamic Behavior of the Transition Zone of an Integral Abutment Bridge Sustainability 14 7 4118.
[30] Railway Technical Research Institute, Design standards for Railway Structures and Commentary (Earth Structures), Tokyo, Japan, 2007.
[31] F. Tatsuoka, M. Tateyama, H. Aoki, and K. Watanabe, "Bridge Abutment Made of Cement-Mixed Gravel Backfill," *Ground Improvement Case Histories: Chemical, Electrokinetic, Thermal and Bioengineering Methods*, pp. 351–399, 2015.
[32] N.R. Administration of P.R. China, TB 10001–2005: Design standards for railway embankments 2005 Beijing, China.
[33] N.R. Administration of P.R. China, TB 1062–2014: Code for design of high-speed railway 2014 Beijing, China.
[34] International union of railways, "UIC 719R: Earthworks and track bed for railway lines," 2008.
[35] K. Liu, Q. Su, P. Ni, C. Zhou, W. Zhao, F. Yue, Evaluation on the dynamic performance of bridge approach backfilled with fibre reinforced lightweight concrete under high-speed train loading, Comput. Geotech. 104 (2018) 42–53, https://doi.org/10.1016/j.compgeo.2018.08.003.
[36] A. Paixão, E. Fortunato, R. Calçada, Transition zones to railway bridges: track measurements and numerical modelling, Eng. Struct. 80 (2014) 435–443, https://doi.org/10.1016/j.engstruct.2014.09.024.
[37] Y. Shan, B. Albers, S.A. Savidis, Influence of different transition zones on the dynamic response of track-subgrade systems, Comput. Geotech. 48 (2013) 21–28, https://doi.org/10.1016/j.compgeo.2012.09.006.
[38] C. Shi, C. Zhao, X.u. Zhang, A. Andersson, Analysis on dynamic performance of different track transition forms using the discrete element / finite difference hybrid method, Comput. Struct. 230 (2020) 106187.
[39] I.G. Giner, A.L. Pita, Numerical simulation of embankment—structure transition design, Proc Inst Mech Eng F J Rail Rapid Transit 223 (4) (2009) 331–343, https://doi.org/10.1243/09544097JRRT234.
[40] Y. Shan, X. Li, S. Zhou, Multi-objective optimisation methodology for stiffness combination design of bridge-embankment transition zones in high-speed railways, Comput. Geotech. 155 (2023) 105242.
[41] X. Lei, L. Mao, Dynamic response analyses of vehicle and track coupled system on track transition of conventional high-speed railway, J. Sound Vib. 271 (2004) 1133–1146, https://doi.org/10.1016/S0022-460X(03)00570-4.
[42] A. Namura, T. Suzuki, Evaluation of countermeasures against differential settlement at track transitions, QR of RTRI 48 (3) (2007) 176–182.
[43] R. Sañudo, M. Cerrada, B. Alonso, L. dell'Olio, Analysis of the influence of support positions in transition zones. a numerical analysis, Constr. Build. Mater. 145 (2017) 207–217, https://doi.org/10.1016/j.conbuildmat.2017.03.204.

[44] M. Wu, Z. Ba, J. Liang, A procedure for 3D simulation of seismic wave propagation considering source-path-site effects: theory, verification and application, Earthquake Engineering Structural Dynamics 51 (12) (2022) 2925–2955.
[45] C. Charoenwong, D.P. Connolly, A. Colaço, P. Alves Costa, P.K. Woodward, A. Romero, P. Galvín, Railway slab vs ballasted track: A comparison of track geometry degradation, Constr. Build. Mater. 378 (2023) 131121.
[46] C. Charoenwong, D.P. Connolly, K. Odolinski, P. Alves Costa, P. Galvín, A. Smith, The effect of rolling stock characteristics on differential railway track settlement: an engineering-economic model, Transp. Geotech. 37 (2022) 100845.
[47] A.C. Lamprea-Pineda, D.P. Connolly, M.F.M. Hussein, Beams on elastic foundations – a review of railway applications and solutions, Transp. Geotech. 33 (2022) 100696.
[48] P. Galvín, A. Romero, J. Dominguez, Fully three-dimensional analysis of high-speed train – track – soil-structure dynamic interaction, J. Sound Vib. 329 (2010) 5147–5163, https://doi.org/10.1016/j.jsv.2010.06.016.
[49] D.P. Connolly, K. Dong, P. Alves Costa, P. Soares, P.K. Woodward, High-speed railway ground dynamics: a multi-model analysis, International Journal of Rail Transportation 8 (4) (2020) 324–346.
[50] T.T. Nguyen, B. Indraratna, A Coupled CFD–DEM Approach to Examine the Hydraulic Critical State of Soil under Increasing Hydraulic Gradient, Int. J. Geomech. 20 (9) (2020) 1–15, https://doi.org/10.1061/(asce)gm.1943-5622.0001782.
[51] J.Y. Shih, D.J. Thompson, A. Zervos, The effect of boundary conditions, model size and damping models in the finite element modelling of a moving load on a track / ground system, Soil Dyn. Earthq. Eng. 89 (2016) 12–27, https://doi.org/10.1016/j.soildyn.2016.07.004.
[52] S. Matias, "Numerical Modelling and Design of Slab tracks - Comparison with Ballasted Tracks," 2014.
[53] C. Cruz and E. Miranda, "A Critical Review of the Rayleigh Damping Model," in *Proceedings of the 16th World Conference on Earthquake Engineering*, 2018.
[54] A. Alipour and F. Zareian, "Study Rayleigh Damping in structures; Uncertainties and Treatments," in *Proceedings of the 14th World Conference on Earthquake Engineering*, 2008.
[55] J.O. Hallquist, LS-DYNA Theory Manual, Livermore Software Technology Corporation, Livermore, California, 2006.
[56] U. Basu, Explicit finite element perfectly matched layer for transient three-dimensional elastic waves, Int. J. Numer. Meth. Eng. 77 (2) (2009) 151–176.
[57] P. Chumyen, D.P. Connolly, P.K. Woodward, V. Markine, The effect of soil improvement and auxiliary rails at railway track transition zones, Soil Dyn. Earthq. Eng. 155 (2022) 107200.
[58] A. Mosleh, P.A. Costa, R. Calçada, A new strategy to estimate static loads for the dynamic weighing in motion of railway vehicles, Proceedings of the Institution of Mechanical Engineers, Part F: Journal of Rail and Rapid Transit 234 (2) (2020) 183–200.
[59] G. Kloosterman, Contact Methods in Finite Element Simulations, University of Twente, The Netherlands, 2002.
[60] M.R. Pajand, M.T. Hakkak, Nonlinear Analysis of truss structures using dynamic relaxation, Int. J. Eng. 19 (1) (2006) pp.
[61] T.D. Akinosho, L.O. Oyedele, M. Bilal, A.O. Ajayi, M.D. Delgado, O.O. Akinade, A. A. Ahmed, Deep learning in the construction industry: a review of present status and future innovations, Journal of Building Engineering 32 (2020) 101827.
[62] A.B. Goktepe, A.H. Lav, Method for optimizing earthwork considering soil properties in the geometric design of highways, J. Surv. Eng. 130 (4) (2004) 183–190, https://doi.org/10.1061/(asce)0733-9453(2004)130:4(183).
[63] W.L. Hare, V.R. Koch, Y. Lucet, Models and algorithms to improve earthwork operations in road design using mixed integer linear programming, Eur. J. Oper. Res. 215 (2) (2011) 470–480, https://doi.org/10.1016/j.ejor.2011.06.011.
[64] Y. Villar, M. Menéndez, Z. Fernández, A. Bernardo, Sustainable earthworks: Optimization with the ICOM method, Energy Rep. 6 (2020) 404–419.